

# Effects of laser shock peening on the mechanisms of fatigue short crack initiation and propagation of AA7075-T651

Sanchez, A. G., You, C., Leering, M., Glaser, D., Furfari, D., Fitzpatrick, M. E., Wharton, J. & Reed, P. A. S.

Author post-print (accepted) deposited by Coventry University's Repository

## Original citation & hyperlink:

Effects of laser shock peening on the mechanisms of fatigue short crack initiation and propagation of AA7075-T651', *International Journal of Fatigue*, vol. 143, 106025.

<https://dx.doi.org/10.1016/j.ijfatigue.2020.106025>

DOI 10.1016/j.ijfatigue.2020.106025

ISSN 0142-1123

Publisher: Elsevier

**NOTICE: this is the author's version of a work that was accepted for publication in *International Journal of Fatigue*. Changes resulting from the publishing process, such as peer review, editing, corrections, structural formatting, and other quality control mechanisms may not be reflected in this document. Changes may have been made to this work since it was submitted for publication. A definitive version was subsequently published in *International Journal of Fatigue*, 143 (2021)] DOI: 10.1016/j.ijfatigue.2020.106025**

© 2021, Elsevier. Licensed under the Creative Commons Attribution-NonCommercial-NoDerivatives 4.0 International

<http://creativecommons.org/licenses/by-nc-nd/4.0/>

Copyright © and Moral Rights are retained by the author(s) and/ or other copyright owners. A copy can be downloaded for personal non-commercial research or study, without prior permission or charge. This item cannot be reproduced or quoted extensively from without first obtaining permission in writing from the copyright holder(s). The content must not be changed in any way or sold commercially in any format or medium without the formal permission of the copyright holders.

This document is the author's post-print version, incorporating any revisions agreed during the peer-review process. Some differences between the published version and this version may remain and you are advised to consult the published version if you wish to cite from it.

# **Effects of Laser Shock Peening on the Mechanisms of**

## **Fatigue Short Crack Initiation and Propagation of**

### **AA7075-T651**

Corresponding author details: Alvaro Sanchez. [Agsal1m17@soton.ac.uk](mailto:Agsal1m17@soton.ac.uk), 07903139355.

Authors: Sanchez AG<sup>1,2</sup>, You C<sup>3</sup>, Leering M<sup>4</sup>, Glaser D<sup>5</sup>, Furfari D<sup>6</sup>, Fitzpatrick ME<sup>4</sup>, Wharton<sup>2</sup>  
J, Reed PAS<sup>1</sup>.

<sup>1</sup>Materials Research Group, Faculty of Engineering and Physical Sciences, University of Southampton, UK

<sup>2</sup>National Centre for Advanced Tribology at Southampton, Faculty of Engineering and Physical Sciences, University of Southampton, UK

<sup>3</sup>College of Energy and Power Engineering, Nanjing University of Aeronautics and Astronautics, Nanjing, 210016, China

<sup>4</sup>Faculty of Engineering, Environment, and Computing, Coventry University, Coventry, UK

<sup>5</sup>National Laser Centre, Council for Scientific and Industrial Research, Pretoria, South Africa

<sup>6</sup>Airbus Operations GmbH

#### **Highlights**

- Laser shock peening performed on AA7075-T651 to improve fatigue performance.
- XRD and incremental hole drilling show deep compressive residual stresses.
- 4-point bend testing and fractography show a change in fatigue regime and large increase in fatigue life.
- Modelling highlights sensitive balance between surface roughness, residual stress and micro-mechanisms of crack initiation.

## List of symbols

LSP	Laser shock peening
7XXX	Seven thousand series aluminium alloys
L	Longitudinal microstructural direction
LT	Long transverse microstructural direction
ST	Short transverse microstructural direction
$S_1$	Compressive residual stress measurement direction parallel to L
$S_3$	Compressive residual stress measurement direction parallel to LT
XRD	X-ray diffraction
SEM	Scanning electron microscope
EDS	Energy dispersive spectroscopy
EBSD	Electron backscatter diffraction
SEI	Secondary electron imaging
BEI	Backscatter electron imaging
SiC	Silicon carbon grit paper
$\Delta K$	Stress intensity factor range
$da/dN$	Crack growth vs number of cycles
$N_{Total}$	Total number of fatigue cycles based on equation 1
$N_{R=0.1}$	Number of fatigue cycles in 0.1 load ratio
$N_{R=0.5}$	Number of fatigue cycles in 0.5 load ratio
Hv	Vickers hardness
$R_a$	Mean roughness
$R_q$	Root mean square roughness
$R_z$	Mean roughness depth
$R_t$	Maximum roughness depth
$R_{sk}$	Skewness
KAM	Kernel average misorientation
CSIR	Council for scientific and industrial research
FE	Finite element
LCF	Low cycle fatigue
HCF	High cycle fatigue

## **Abstract**

A laser shock peening (LSP) treatment was performed on AA7075-T651 for maximum fatigue improvement. Surface and microstructural characterisation techniques (micro-hardness, SEM-EBSD, contact-profilometry) showed LSP surface modification was limited, and LSP generated deep compressive residual stresses above -300MPa. Fatigue testing showed a two-order magnitude increase in overall life, due to the mechanism of crack initiation changing from surface second-phase particles to subsurface crack initiation dependent on the local stress field. Modelling highlights the sensitive balance between surface roughness (including LSP-induced pits) and residual stress on the micro-mechanism of crack initiation, and how this can be used to maximise fatigue life extension.

### **Keywords:**

Aluminium alloys, fatigue initiation, micromechanics, surface flaws.

# 1. Introduction

Laser shock peening (LSP) is a relatively new form of mechanical surface treatment. It is similar to shot peening in terms of objective: Imparting beneficial compressive residual stresses to the surface and near surface of the material. Unlike shot peening, LSP uses high power laser pulses to ionise the surface into a high pressure plasma within a transparent inertial confinement medium (typically water). The confined plasma generates a Giga Pascal (GPa) magnitude pressure, which transmits shock waves into the metal surface, causing constrained localised surface and subsurface plastic deformation, generating compressive residual stresses [1][2][3]. A sacrificial coating such as black tape or aluminium foil may be used as a thermo-protective overlay to preserve the surface integrity of the target.

The manufacturing benefits of using LSP surface treatment over shot peening are the accuracy and precision that LSP allows [1][4][5]. In addition, LSP has shown improvements in the maximum level and depth of compressive residual stress achieved below the surface [1][4], a beneficial decrease in detrimental surface modification and improvement in fatigue life in comparison to shot peening [1][6][7]. Therefore, LSP is now a technology that is expanding in use in aerospace and other industries.

Aluminium alloys are used extensively in the aerospace industry and, naturally, LSP treatment is seen as a promising method for improving fatigue life of aerospace aluminium components [1]. The effectiveness of LSP treatment on fatigue life depends on the combination of laser parameters chosen for a specific type of material, with the aim to minimise surface modification (particularly roughness) and maximise compressive residual stress, which in turn maximises fatigue life. Nevertheless, there are several LSP parameters to consider (power density, spot shape, spot overlap, energy, etc.) and each material responds differently to these. Thus knowing the appropriate combination of LSP parameters prior to treatment is important for each specific material [1][5].

For a specific LSP treatment, different aluminium alloys (and tempers) will achieve different levels of residual stresses. Several studies have shown this variation in residual stress achieved as a function of LSP treatment parameters and the alloy temper, in 2XXX alloys [8][9][10], AA7075 [5][6] [11] and other 7XXX alloys [12][13]. As well as varying residual stress, varying levels of surface roughness [6][14][15][16] [17] and hardening of the surface [18][19][15] after LSP treatment, have been seen in previous studies of aerospace grade aluminium alloys, including 7XXX alloys [6][20][21] [22]. It has also been shown that, unlike shot peening, appropriate LSP treatment generates limited increase in surface roughness of aluminium alloys, whilst generating similar or higher levels of compressive residual stress to shot peening [6][21][22]. In terms of surface hardening of aluminium alloys by LSP, some papers have found hardening in all tempers [23][10], whilst others have found no hardening, particularly in peak aged alloys [6][21].

Considering the different LSP treatments and their different effects on each alloy and temper, the effectiveness of LSP treatment on fatigue performance would be expected to vary considerably. The available literature indicates varying improvements in LSP treated 2XXX alloys [8][9], [10] and 7XXX alloys [12][4][6][17]. In the case of AA7075, studies show fatigue life improvements have varied from 11% to over 100% compared to untreated samples [4][21][24][25]. In addition, some studies have seen changes in the mechanisms of crack initiation. Zhang *et al.* [17] and Gao[22] found LSP-treated AA7075-T6 and AA7050-T7451 saw fatigue life improvements attributed to a change from surface (for untreated) to sub-surface crack initiation. Nevertheless, this change in crack initiation mechanisms has not been seen in most LSP treated aluminium alloy studies surveyed. Overall, it is unclear the extent to which roughness, hardness and the level of LSP residual stress, respectively, contribute to the overall fatigue life improvement, and how each of these influence the possible change in micro-mechanisms of crack initiation and propagation in aluminium alloys after LSP treatment.

The aim of this study was to perform a representative LSP treatment with minimal surface modification on aerospace grade AA7075-T651 to improve fatigue life. Then based on this, to understand how, and to what extent, the LSP generated residual stress, and the modified surface (hardness and roughness), will each influence changes in the micro-mechanisms of short crack fatigue initiation and growth in aerospace grade AA7075-T651. This experimental understanding is linked to modelling the effect of the residual stress distribution and how this interacts with surface roughness features to determine fatigue life to inform and validate this mechanistic understanding. A validated model based on this mechanistic understanding will provide a sound basis for predicting LSP fatigue improvements and direct LSP optimisation.

## 2. Experimental Methods

A number of surface and microstructural characterisation tools, residual stress assessment tools and fatigue testing and analysis methods were used to understand how LSP treatment modifies the surface and near-surface microstructure of AA7075-T651, and how this, together with the LSP-induced compressive residual stresses, has changed fatigue performance and the underlying mechanisms of crack initiation and propagation.

### 2.1. Materials and LSP treatment

The material in this study was sourced from a 40 mm thick AA7075 plate with T651 temper. According to the literature its properties are as follows: A tensile strength of 572 MPa, yield strength of 503 MPa, Vickers hardness of approximately 175 and fracture toughness of 20 to 29 MPa $\sqrt{m}$  depending on the microstructural plane loaded [26].

All samples tested in this study were removed from an AA7075-T651 plate, at T/4 (one quarter thickness), with the top surface (the surface tested) in the L-LT plane (See Figure 2-1).

Samples for microstructure characterisation were cut to a 5 mm × 5 mm area, mounted and polished to 1 µm surface finish with samples taken from the L-LT, L-ST and LT-ST plane. These were etched using Keller's reagent (2 ml HF, 3 ml HCl, 5 ml HNO<sub>3</sub>, 190 ml H<sub>2</sub>O).

Samples were cut into fatigue bend bars with the dimensions shown in Figure 2-1. This was a variation of the sample geometry used by Luong and Hill [27], which was shown to be effective for fatigue testing of LSP samples, the chamfered sides avoiding discontinuities in the LSP process. The bend bar samples were cut from the longitudinal – long transverse (L-LT) plane of the AA7075 plate. Prior to LSP treatment, all bend bars were mechanically ground with 1200 SiC grit paper. A block of 77 mm × 40 mm area × 30 mm depth was also LSP treated with the same processing parameters as the bend bars.

Roughness measurements and hardness tests were performed on the bend bars post fatigue test, at least 20 mm away from the fracture surface, where the LSP-induced residual stress is not expected to have been affected by the fatigue testing and fracture processes. A small number of hardness measurements were also performed on samples of 5 mm × 5 mm area and 30 mm depth, taken from the LSP block mentioned above.

Laser Shock Peening was performed at the Council for Scientific and Industrial Research (CSIR), South Africa. The LSP configuration used a frequency doubled Nd:YAG laser (Thales SAGA HP) to deliver parameters shown in Table 2-1. A thin water layer was used to achieve inertial confinement, and a black tape (around 100 µm thick with a 30 µm adhesive) was used as a sacrificial overlay. Spot overlap is achieved by sample motion in a conventional (X-Y) raster pattern by scanning (in the LT direction) and stepping (in the L directions) to achieve equal spot overlap (of 48.4% in the LT and L directions). To homogenise any periodic features such as residual stress between sequential overlays [7], subsequent sequential layers of LSP were applied with a spot offset (one third of the spot-to-spot distance to achieve 48.4% overlap).

In total, three sequential applications of LSP were applied (each with a new tape) to achieve a total coverage of 5 spots per mm<sup>2</sup>. The samples were peened across the top surface and the chamfered sides, as shown in Figure 2-1, to avoid crack formation outside the top flat surface.

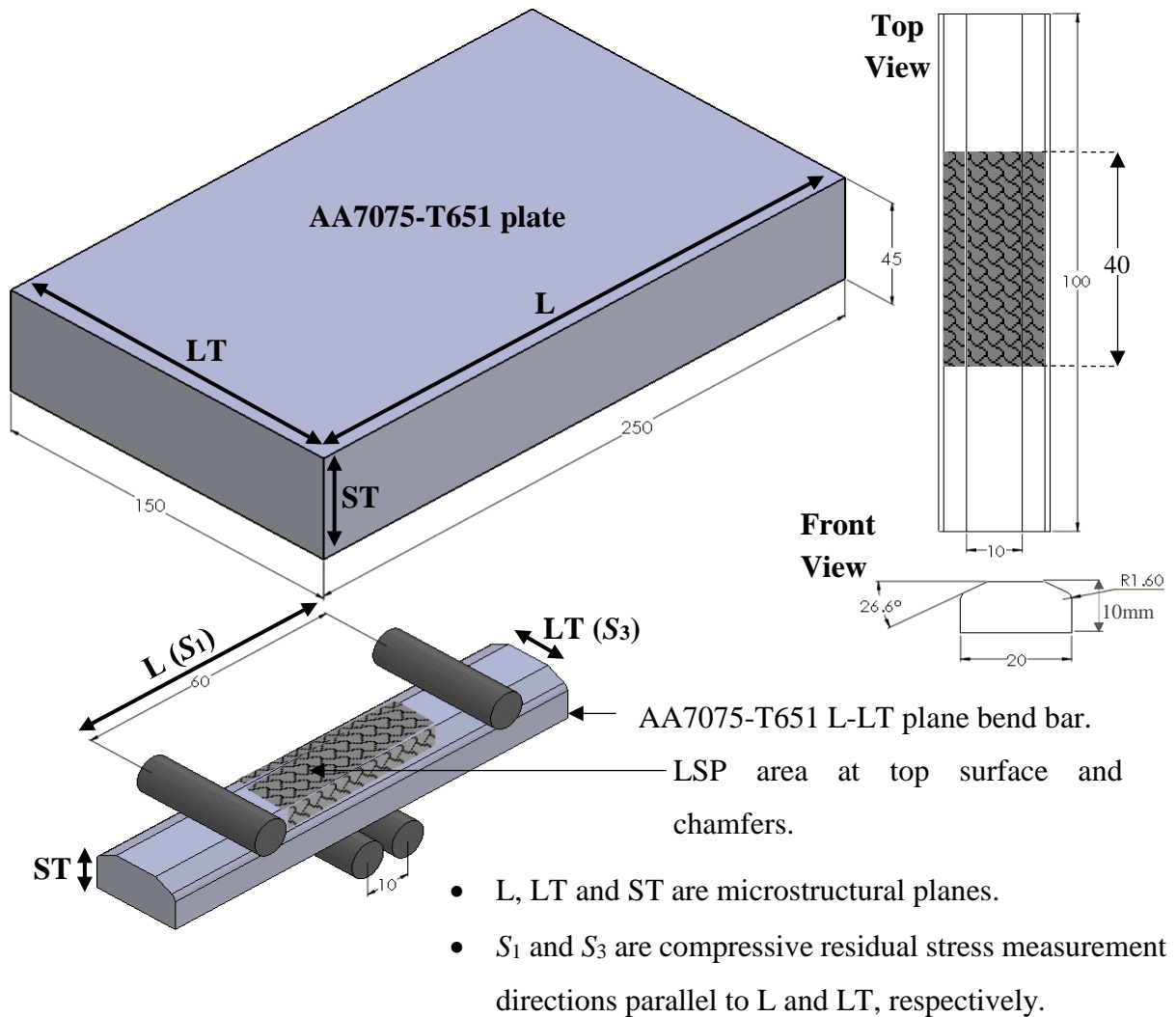


Figure 2-1.- Schematics of AA7075-T651 plate and LSP sample geometry and LSP area.

Table 2-1 – LSP parameters

Parameter	Value
Power Density / GW.cm <sup>-2</sup>	4
Wavelength / nm	532
Spot Shape	Circular
Dimension / mm	1.5 dia.

Spot offset / mm	0.258
Spot overlap / %	166.7 spots/cm <sup>2</sup> ( $\approx$ 48.4%)
Energy / mJ	364
Sacrificial coating	Black vinyl tape

## 2.2. Surface and microstructural characterisation

A Talysurf contact profilometer was used to perform roughness testing to ISO4287 standard. For micro-hardness, an FM-300 Microhardness Tester machine was used, with a 0.5 kg-f load and 30 seconds hold time. Ten to fifteen readings were taken from each sample. A baseline bend bar and an LSP bend bar, as received, were tested. A third sample, a 5 mm  $\times$  5 mm cross section cut from an LSP block (see section 2.1) was also characterised. It is well known that removing material from a component that contains residual stresses will relieve these, and the larger the amount of material removed the greater the stress relief [28]. Thus, it is assumed hardness testing on this 5mm  $\times$  5mm cross-section sample would give hardness values based mostly on microstructural changes, with reduced effects from any remaining residual stress.

Baseline and LSP samples were characterised using an Olympus BX41M-LED, Alicona InfiniteFocus™ focus variation microscope and a JEOL JSM-6500F scanning electron microscope (SEM). The focus variation microscope was used to generate 3D surface topography images of the bend bar surfaces. The SEM was used for secondary electron imaging (SEI) and backscatter electron imaging (BEI), including energy dispersive X-ray spectroscopy (EDS) and electron backscatter diffraction (EBSD). Voltages used for imaging (SEI and BEI), EDS and EBSD were 10, 15 and 20 keV, respectively.

For EBSD, cross sections of the baseline and LSP treated material (LT-ST plane) were scanned. Prior to EBSD, they were mechanically polished up to a 3  $\mu$ m surface finish with diamond suspension, followed by electropolishing. See Table 2-2 for more information. For EBSD, each scan was 145  $\mu$ m long by 100  $\mu$ m wide in dimensions. These scans were repeated progressively

to 770  $\mu\text{m}$  below the laser shock peened surface. Oxford Instruments Tango software was used to analyse the grain misorientation profile of the baseline and LSP cross-section. Grains are classified as deformed if the average misorientation between all points within a grain is above 1 degree. Grains are classified as substructured if the average misorientation angle of a grain is 1 degree, but the misorientation angle between any two points within the grain is higher than 1 degree. Finally, grains are classified as recrystallised if the average misorientation angle of the grain is below 1 degree [29]. EBSD data was processed in Matlab using MTEX Toolbox [30] to calculate the kernel average misorientation in the LSP cross-section, giving a quantitative understanding of the plastic deformation caused by LSP treatment.

*Table 2-2 – Electropolishing parameters*

<b>Electropolishing parameters</b>	
Electrolyte	Two parts methanol, one part nitric acid
Voltage	25 – 30 Volts
Bath temperature	25 – 35 °C
Time	2 – 5 seconds

### 2.3. Residual stress analysis

X-ray Diffraction (XRD) and incremental centre hole drilling were used in a complementary manner, to assess the residual stresses present in the LSP samples at and below the surface [31][32]. The XRD measurements were completed with a Stresstech Xstress diffractometers on an articulated robot, which uses the  $d$  vs.  $\sin^2\psi$  technique to determine the stress. A chromium X-ray source was used with a 1mm diameter collimator and count time of 20 seconds at each of the fourteen tilt locations evenly spaced between  $-45/45^\circ$ . Additionally, a  $\pm 2.5^\circ$  tilt angle was used at each measurement location to increase the number of sampled grains. The  $0^\circ$  and  $90^\circ$  measurement angles were aligned with the longitudinal ( $S_1$ ) and transverse ( $S_3$ )

directions of the samples (See Figure 2-1). The measurement distance was calibrated based on a stress free aluminium powder sample and was set at a calibration stress of  $-22 \pm 10$  MPa ( $0^\circ$  direction) and  $-14 \pm 11$  MPa ( $90^\circ$  direction).

The hole drilling measurements were made with a Stresscraft three axis drilling device. A drilling feed rate of  $10 \mu\text{m}/\text{second}$  was used with a 1.2 mm diameter drill on a 0.3mm orbital eccentricity to create a hole diameter of 1.8-2.0 mm. The measurements were created with twenty-three surface biased (smaller increments near the surface) incremental depths using an orbital drilling motion. The measurements were taken in the centre of the LSP region on the bend bar sample. Strain readings were taken up to 1.024 mm from the surface in the longitudinal ( $S_1$ ) and transverse ( $S_3$ ) directions of the samples.  $S_1$  was also the direction of loading in 4-point bend bar fatigue tests (See Figure 2-1). As it is well known that centre hole drilling measurements at, or very close, to the surface can be inaccurate [31][32], only values from  $16 \mu\text{m}$  below the surface are shown.

#### 2.4. Fatigue testing

A servo-hydraulic Instron machine was used for four-point bend testing. The 4-point bend test was performed at 20 Hz frequency, with a load ratio of 0.1. The load setup is shown in Figure 2-1.

Post LSP treatment some bend bars were tested as received (1200 SiC grind followed by LSP treatment), whilst others were polished, post-LSP, to  $1 \mu\text{m}$  surface finish. In total, twelve baseline and eight LSP fatigue tests were performed.

A number of samples were initially tested below yield stress values to compare fatigue performance and analyse mechanisms of crack initiation and growth in a predominantly elastically loaded sample, with limited plastic strain ranges.

A small number of baseline and LSP samples were also tested at above yield stress values to understand how the LSP compressive residual stresses beneficial effects may change due to

higher subsequently applied plastic strain ranges. Overall, for both baseline and LSP tests, the nominal stress ranges (derived from beam theory) used for testing varied from 360 MPa to 595 MPa.

Two methods were used to assess crack propagation: The replica method and the beach marking method. The replica method consists of using ready-made replica material Struers F5. This material is applied during intermittent fatigue cycling of samples to obtain a visual record of the sample top surface and creating a series of snap shots of surface crack initiation and growth processes throughout the sample lifetime. After application of replica to the surface, it takes 20 minutes to harden and capture the sample's surface to 1  $\mu\text{m}$  resolution. This replica can subsequently be observed using optical microscopy. Successive crack lengths are measured and used to calculate crack growth rate  $da/dN$  versus stress intensity factor ( $\Delta K$ ).

For some LSP samples, the replica method was not effective in monitoring crack behaviour due to subsurface crack initiation and growth. In this case, the beach marking method was used. Instron wave matrix was used to set up a regime where the load ratio was varied from  $R = 0.1$  to  $R = 0.5$ , or  $R = 0.1$  to  $R = 0.9$  between blocks of cycling. This variation in load ratio was performed by increasing the minimum load, keeping the maximum load, and therefore  $K_{\text{max}}$ , constant during the whole test. The number of cycles for each load ratio was chosen based on expected total life and via experimental trials. For the 'R=0.1 to R=0.5' tests, fatigue life is presented as an estimate with error bars. The estimated life ( $N_{\text{Total}}$ ) is equal to the cycles under 'R = 0.1' ( $N_{R=0.1}$ ) plus a third of the cycles under 'R=0.5' ( $N_{R=0.5}$ ).

*Equation 1*

$$N_{\text{Total}} = N_{R=0.1} + \left[ \frac{N_{R=0.5}}{3} \right]$$

This is based on the Walker equation used for AA7075-T651 by Dowling et al [33], and a set of AA7075-T651 uniaxial data reported in [34], to estimate fatigue life for different load ratios. One fatigue bend bar was tested at  $R = 0.5$  only, to confirm if this estimate is valid. This fatigue

life estimate approach was also assumed for the LSP bend bars tested. Error bars are also presented to show the minimum fatigue life ( $N_{R=0.1}$ ) and the maximum fatigue life ( $N_{R=0.1} + N_{R=0.5}$ ). For tests performed with variation of  $R=0.1$  to  $R=0.9$ , the number of cycles at  $R=0.1$  ( $N_{R=0.1}$ ) is presented as total life, assuming a very limited contribution by loading at  $R = 0.9$ .

## 2.5. Fractography

Optical microscopy and scanning electron microscopy were used to analyse fracture surfaces of fatigue samples, for both baseline and LSP samples. The SEM was used at an accelerating voltage of 10 - 15 KeV and a working distance at or below 10 mm. SEM microscopy, Fiji processing [35], and fatigue data (number of cycles and load ratio) captured by Instron® Wavematrix were used to measure crack size and calculate crack growth versus  $\Delta K$ .

Secondary electron imaging (SEI) and backscattered electron imaging (BEI) were used for surface imaging, as well as EDS to obtain semi-quantitative data of chemical composition of bulk material and second phase particles.

### 3. Results

#### 3.1. Material characterisation

Figure 3-1 is a 3D representation of the material studied, showing a typical AA7075-T651 microstructure. The three microstructural planes, L-LT, L-ST and LT-ST are shown. The L direction is the rolling direction, resulting in anisotropic grains, in the shape of elongated pancakes. The grains are shortest in the ST direction and longest in the LT direction.

The dark features, varying in size from 1 to 10s of  $\mu\text{m}$ , are known as coarse particles, or coarse intermetallics. Semi-quantitative SEM-EDS of these features suggest most of these are  $\text{Al}_7\text{Cu}_2\text{Fe}$  and  $\text{Al}_{23}\text{Fe}_4\text{Cu}$ , with occasional  $\text{Mg}_2\text{Si}$  (See Figure 3-1).

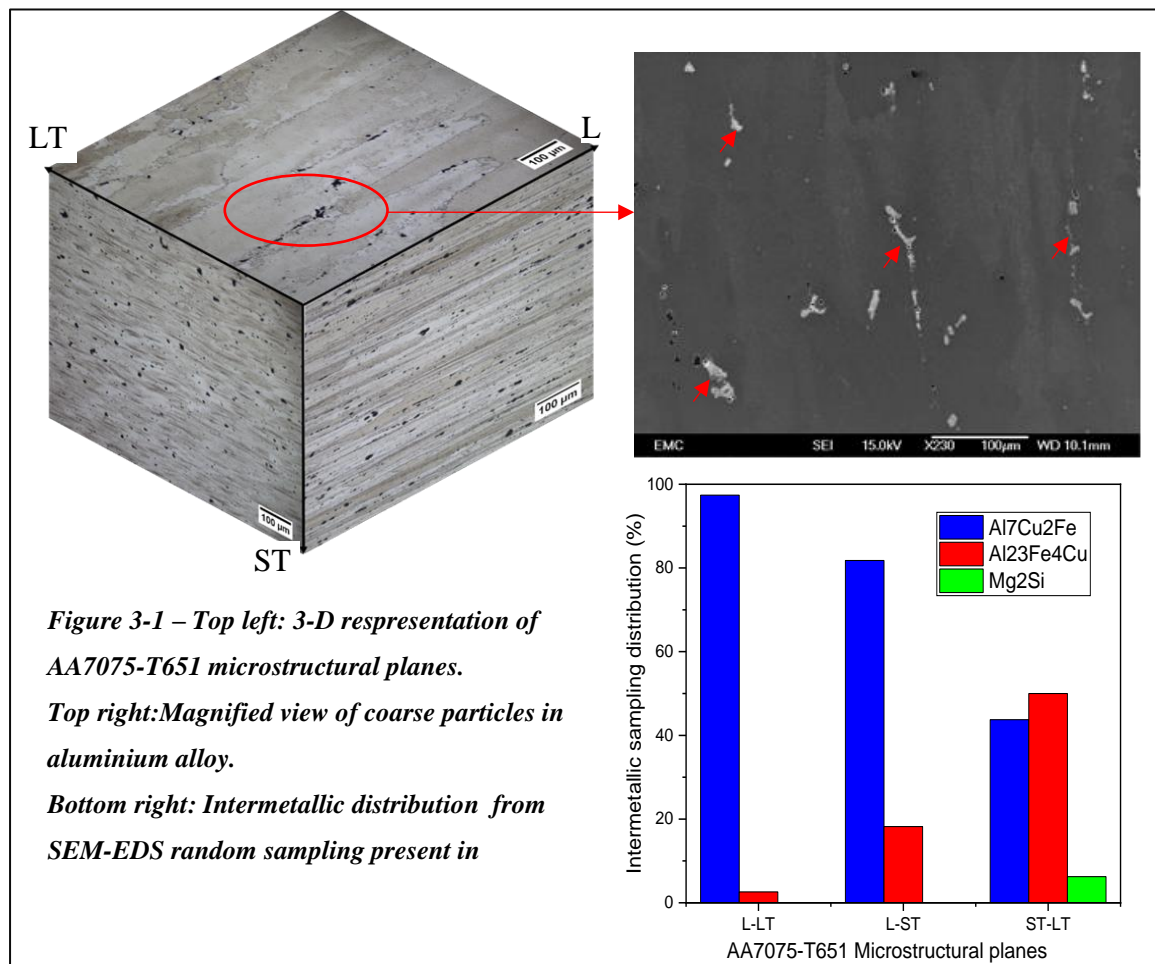


*Figure 3-1 – Top left: 3-D representation of AA7075-T651 microstructural planes.*

*Top right: Magnified view of coarse particles in aluminium alloy.*

*Bottom right: Intermetallic distribution from SEM-EDS random sampling present in*

### 3.2. Residual stresses

The incremental centre hole drilling data in Figure 3-2 shows compressive residual stresses, in both longitudinal ( $S_1$ ) and transverse directions ( $S_3$ ), of up to  $-340$  MPa, found at approximately  $16 \mu\text{m}$  below the surface. The compressive residual stresses then progressively decrease going further into the depth, down to  $-50$  MPa, at approximately  $1.024$  mm below the surface. XRD surface measurements, in **Error! Reference source not found.**, show compressive residual stresses, at the surface, of between  $-330$  MPa and  $-110$  MPa. Overall, the values suggest the highest compressive residual stresses are at, or near, the surface and steadily decreases down to at least  $1$  mm below the surface. When comparing this to the yield stress of the material, of  $503$  MPa, residual stress of up to  $-330$  MPa are expected beneficially increase fatigue life by reducing mean stress levels experienced in the near surface region.

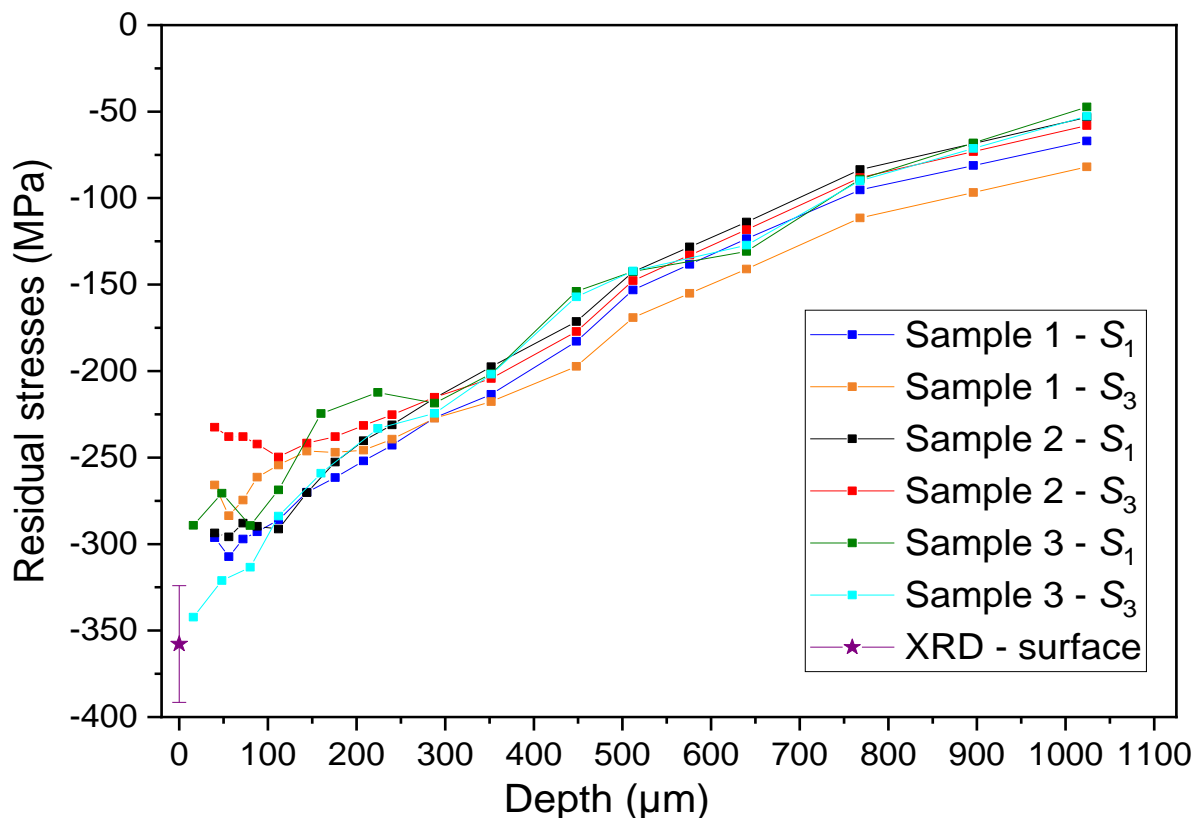


Figure 3-2 - Centre hole drilling data for LSP samples.  $S_1$  in the longitudinal direction,  $S_3$  in the transverse direction.

### 3.3. Surface modification

Hardness tests on ‘as received’ samples show a clear difference between baseline and LSP samples. According to Figure 3-3, as received LSP samples’ average micro-hardness is 188 Hv, a 11% increase compared to baseline, which had an average hardness of 170 Hv. The average hardness for “cut” LSP (residual stresses relieved) is 175 Hv, close to what is seen for the baseline.

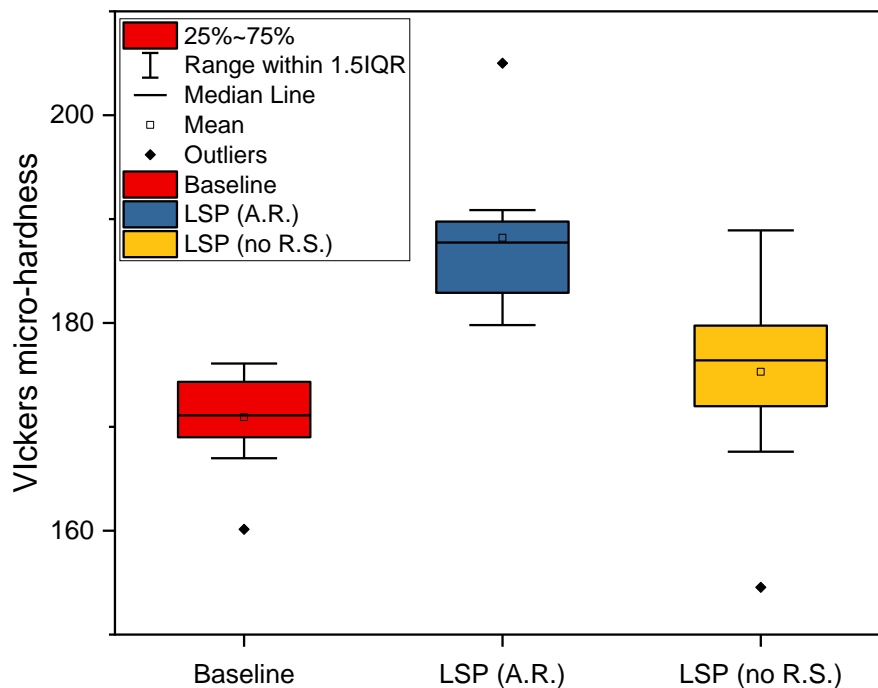


Figure 3-3 – Vickers micro-hardness measurements of baseline LSP samples.

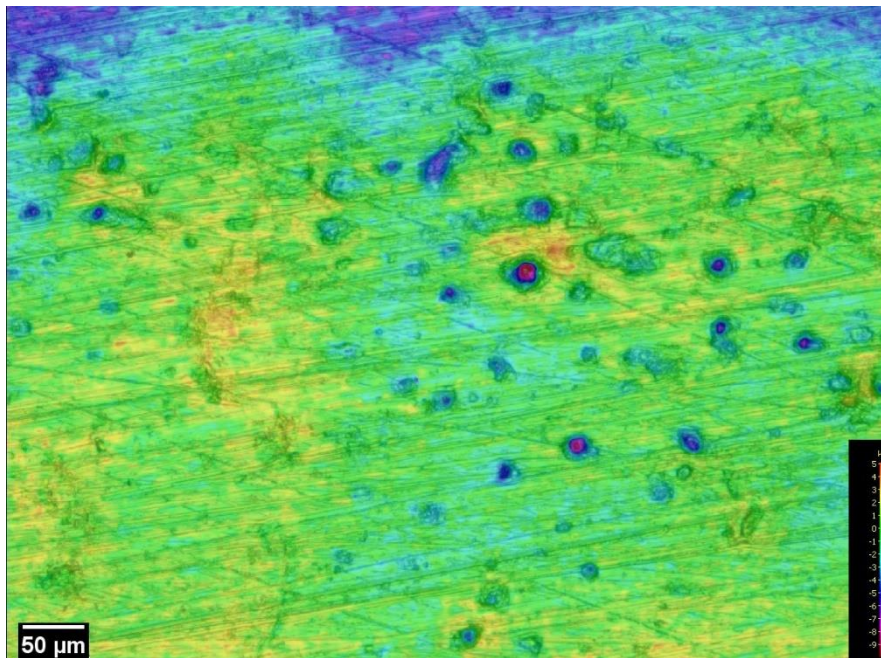
Roughness values are shown in Table 3-1. For each roughness parameter (except for  $R_{sk}$ ) there is roughly a doubling ( $R_z$ ,  $R_t$ ) or tripling ( $R_a$ ,  $R_q$ ) of values from baseline surfaces to LSP surfaces. Nevertheless, these values are in the same order of magnitude. Overall, it suggests the LSP treatment has caused a small amount of surface roughness modification.

Table 3-1 – Average roughness measurements for baseline and as received LSP.

Roughness parameter	Baseline (1200 SiC grind)	LSP
$R_a$ ( $\mu\text{m}$ )	0.23	0.76
$R_q$ ( $\mu\text{m}$ )	0.29	0.90
$R_z$ ( $\mu\text{m}$ )	1.62	3.69

<b><math>R_t</math> (<math>\mu\text{m}</math>)</b>	2.64	5.52
<b><math>R_{sk}</math></b>	-0.10	-0.11

The LSP process also generated a small number of LSP-process pits. A small sampling of bend bar surfaces, using variable focus microscopy, showed LSP generated pits of 2 – 10  $\mu\text{m}$  depth. Although the number of pits per area is random, it appears to be low. In some images there were indications the pits were aligned with the edges of the ablative layer (black vinyl tape). See Figure 3-4.



*Figure 3-4 – An example of a bend bar surface with pits generated by LSP process. Number of pits per area differs greatly but is generally considered low. Captured by variable focus microscopy.*

### 3.4. Microstructure analysis

EBSD recrystallization maps and graphs for baseline and LSP cross-sections (LT-ST microstructural plane) are shown in Figure 3-5 and Figure 3-6, respectively. The recrystallisation analysis shows there has been a significant increase in deformed grains compared to baseline AA7075-T651. The baseline material appears to contain up to 30 – 35% retained deformed grains, which are expected to remain due to rolling during the manufacturing

process. The LSP samples however contain up to 55% deformed grains, a significant increase in grain deformation levels. The largest concentration of deformed grains in the recrystallisation map are at or near the surface. The percentage of deformed grains clearly decreases progressively moving away from the surface. Scans of the LSP LT-ST cross-section at 140  $\mu\text{m}$  below the surface, or even further away, show similar percentage grain deformation as seen in the baseline material. Kernel average misorientation data shown in Figure 3-6 indicates the grain deformation is up to 100  $\mu\text{m}$  under the surface, with the first 50  $\mu\text{m}$  having the highest deformation. This grain deformation reflects the local microstructural change caused by LSP that has induced compressive residual stresses.

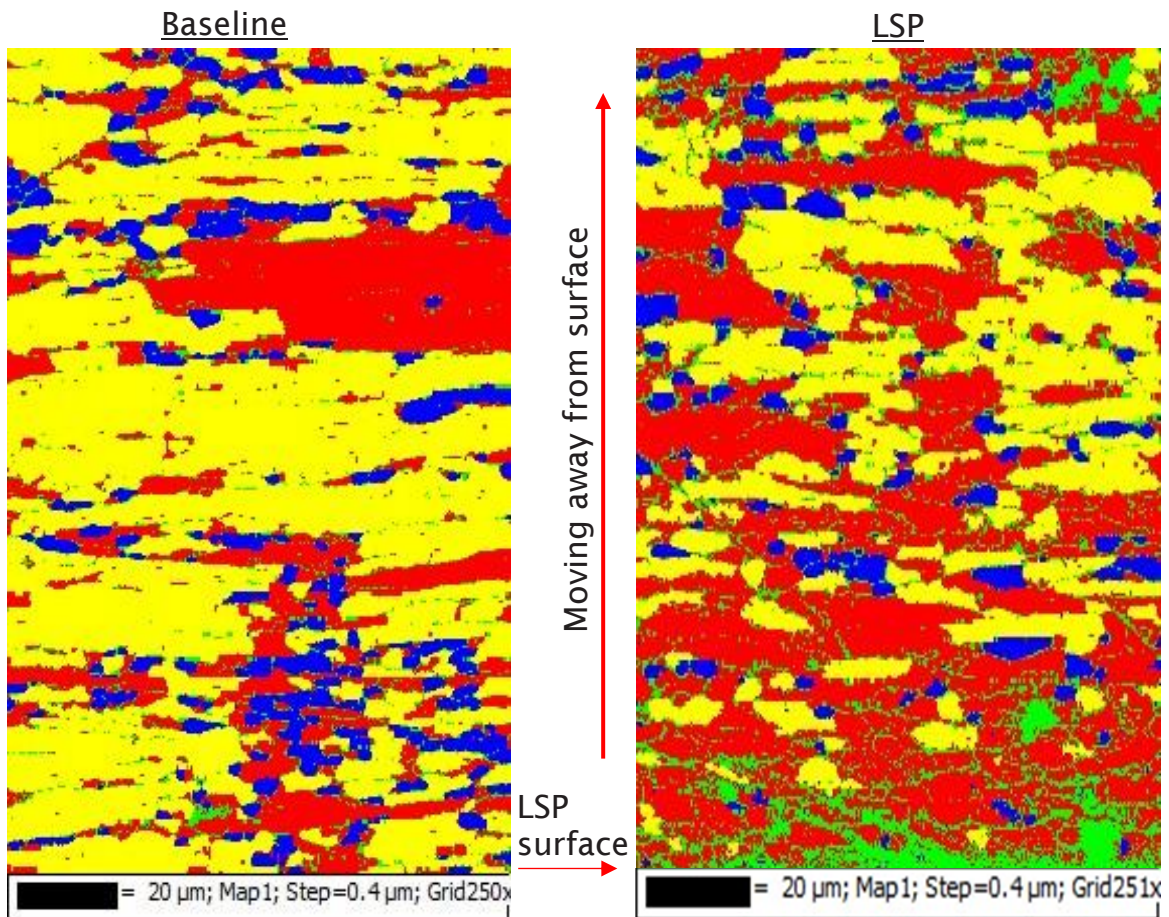


*Figure 3-5 – EBSD maps of samples cross-sections, LT-ST plane. Surface at the bottom, upwards going away from surface. Left: Baseline. Right: LSP.*

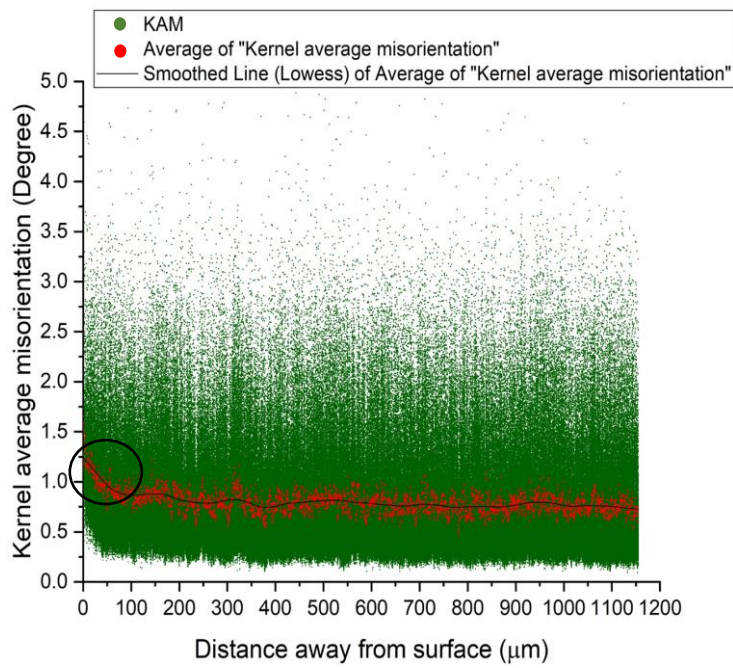
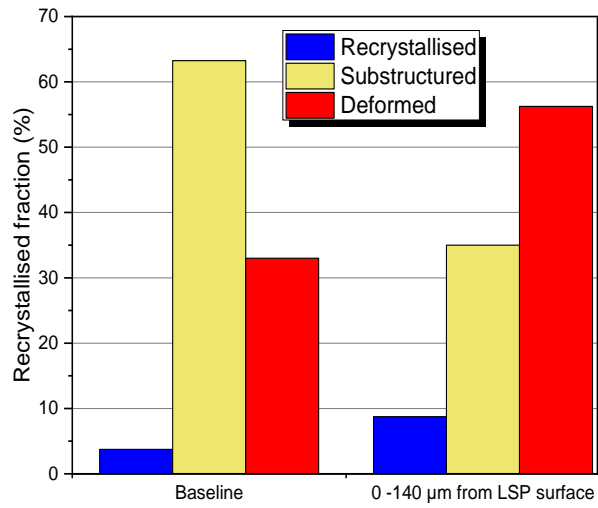


**Figure 3-6 – Top: Recrystallised fraction graph of baseline and LSP surface for LT-ST cross sections: 0 – 140 μm away from surface. Bottom: Kernel average misorientation vs. distance away from LSP surface.**

### 3.5. Fatigue testing

Figure 3-7 shows all the fatigue tests performed in an S-N curve. Generally, fatigue data from baseline bend bar tests fall within the expected scatter of the data reported in the literature [36]. Baseline tests at 407 MPa stress range have fatigue life of  $2 - 6 \times 10^4$  cycles. Data points with an error bar are tests performed using the beach marking method. The fatigue life error bars represent the variation of fatigue cycle counting as mentioned in section 2.4.

The LSP bend bars, 'as received' and 1  $\mu\text{m}$  polished, tested at 407 MPa applied stress range, failed at  $1 - 3 \times 10^6$  cycles, a two orders of magnitude increase in total life. Fatigue lives of LSP 'as received' and 1  $\mu\text{m}$  polished bend bars tested at 407 MPa stress range are in the same order of magnitude. There is one exception, where an 'as received' bend bar failed at  $10^5$  cycles. The causes of this are explored in more detail in section 3.6.

As the stress range at which samples are tested is increased by steps of approximately 50 MPa, the  $10^6$  cycles fatigue life is maintained until the stress range reaches 490 MPa. At this point fatigue life sees a significant drop, to  $10^5$  cycles. A further increase to 540 MPa and 595 MPa stress range (note this is above AA7075-T651 yield stress of 503 MPa) produces another large drop in fatigue life, down to  $10^4$  cycles. These values are now similar to baseline samples tested in the 407 MPa stress range.



As mentioned in section 3.5 there was one exception to the above results. One ‘as received’ LSP bend bar tested at 407 MPa failed at  $10^5$  cycles, not  $10^6$ . The fracture surface, Figure 3-8, show that the crack initiation site is not the same as other LSP fatigue tested samples previously shown. As shown in Figure 3-9, the crack initiation site is from a surface pit of 12  $\mu\text{m}$  depth and approximately 20  $\mu\text{m}$  width.

The fatigue bend bar tested at 490 MPa, which also saw a drop in fatigue life to  $10^5$  cycles, exhibited crack initiation from a pit located at the chamfer, as shown in Figure 3-8(g)(h). All LSP bend bars fatigue tested at 545 and 595 MPa failed from initiation at the top surface. As seen in Figure 3-8(i)(j), all crack initiation sites were at coarse particles, similar to baseline behaviour. SEM-EDS analysis confirmed these crack initiating particles were  $\text{Al}_7\text{Cu}_2\text{Fe}$ .

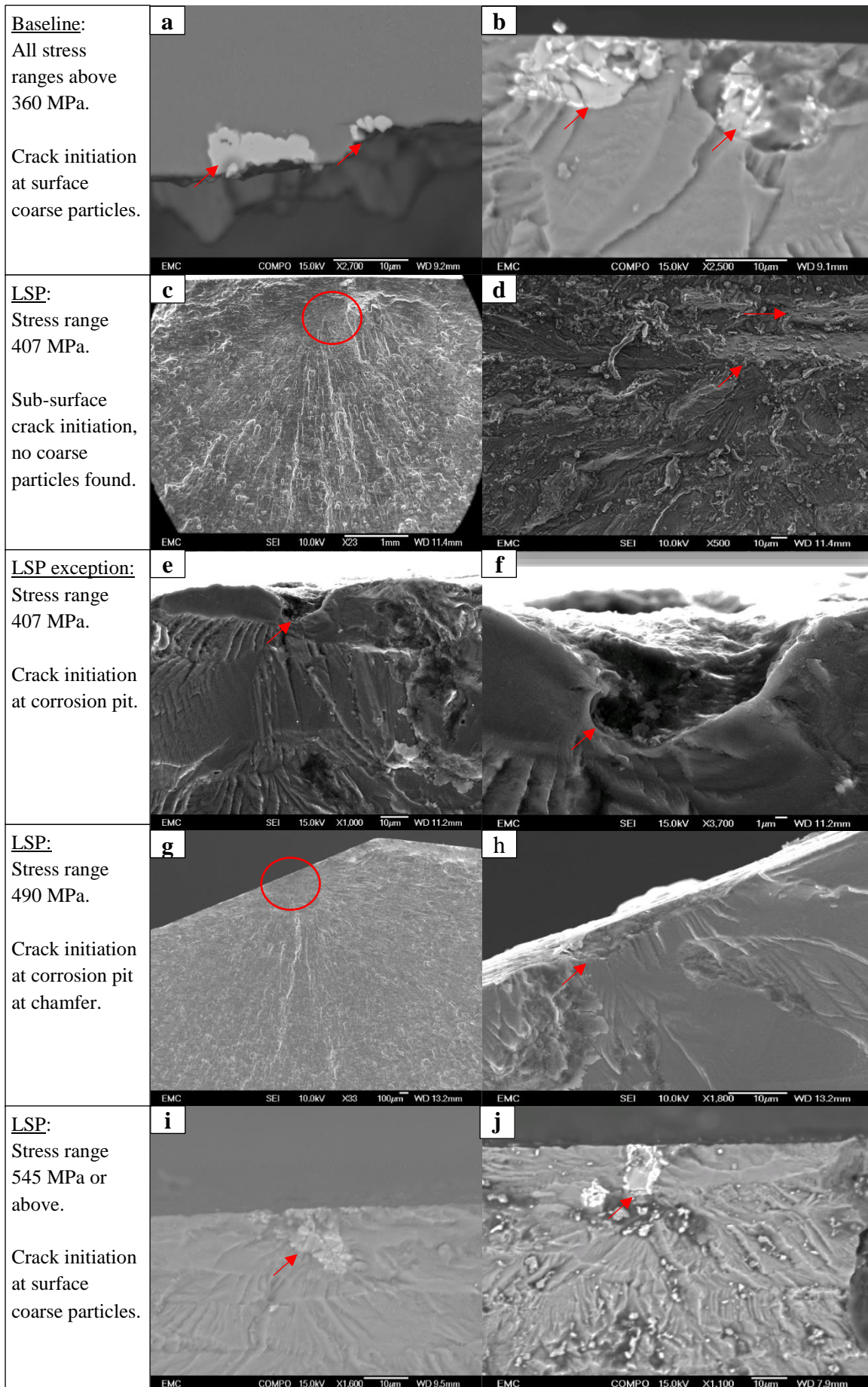
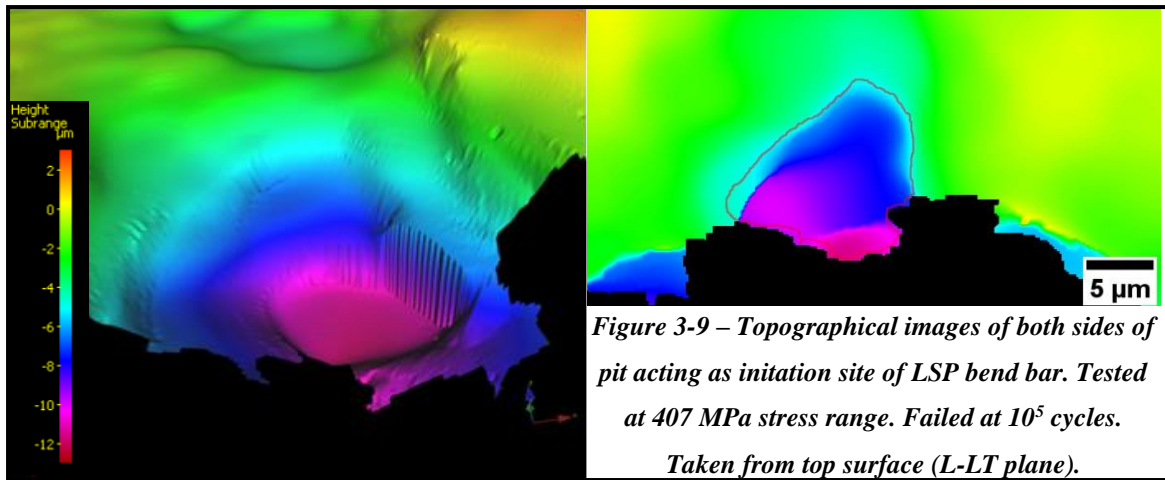


*Figure 3-8 – Low and high magnification images of crack initiation sites for different fatigue test conditions. a-b: All baseline tests. c-d: LSP tests at 407 MPa stress range. e-f: One LSP test at 407 MPa which was an exception to the previous tests. g-h: LSP test at 490 MPa stress range. i-j: LSP tests at or above 545 MPa stress range.*



### 3.7. Crack propagation

Crack propagation information was obtained effectively from the baseline fatigue bend bars using the replica method. Crack propagation data capture from LSP bend bars using beach marking had mixed results. LSP bend bars tested at maximum stress levels above yield stress produced clearer beach marking, leading to a larger number of data points. LSP bend bars tested at maximum stress levels below yield stress yielded limited data due to limited beach marking results.

The crack propagation rate vs.  $\Delta K$  data, shown in Figure 3-10, suggests there is no clear difference in crack propagation rate between baseline and LSP fatigue tests. Furthermore, Figure 3-11 indicates LSP at high cycle fatigue shows crack initiation time is markedly higher than that of baseline samples when comparing applied stress range of 400 MPa. The beneficial effect of LSP compressive residual stress on crack initiation decreases as the applied stress is increased, as seen by the decreased initiation time in the LSP transition sample (490 MPa) and LSP low cycle fatigue samples (above 540 MPa).

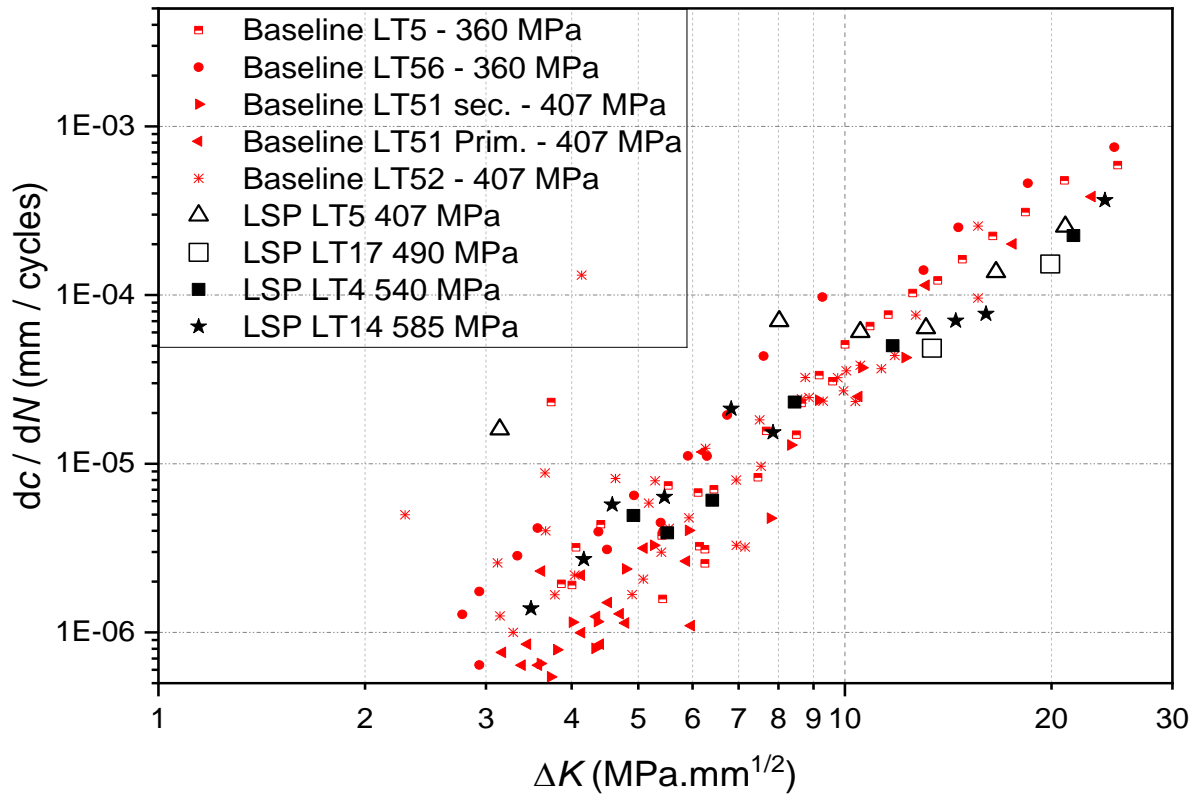


*Figure 3-10 – Crack growth data vs. stress intensity factor for baseline and LSP fatigue tested samples. This includes crack propagation data captured by replica method and the beach marking*

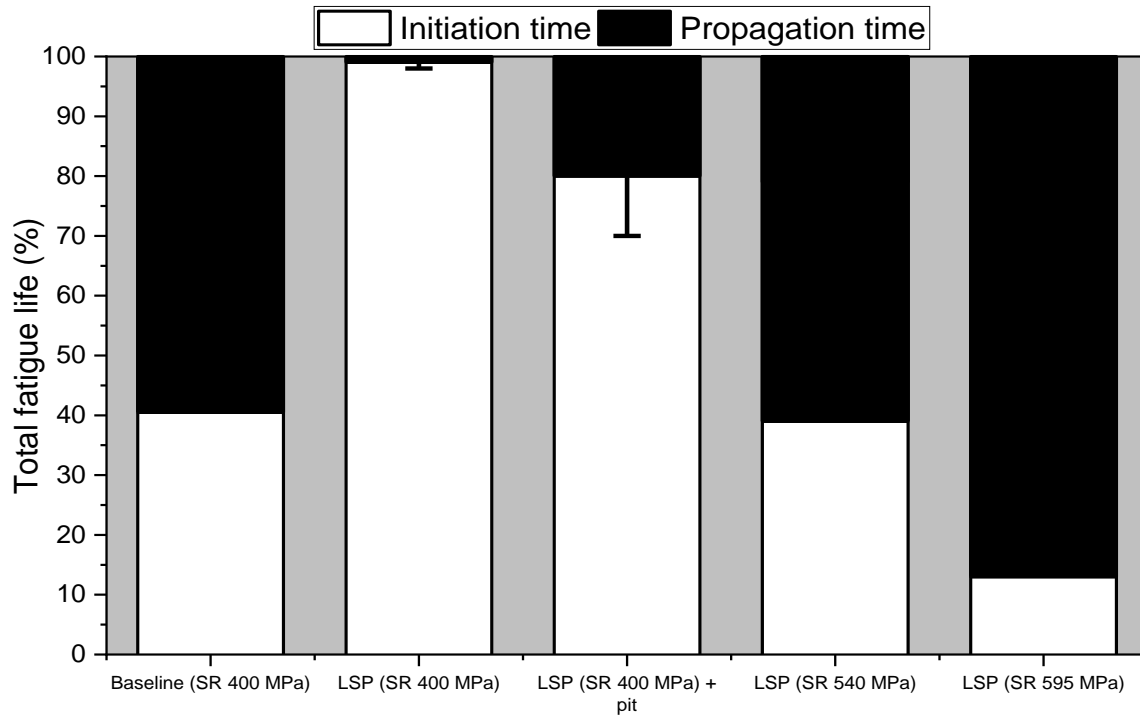


**Figure 3-11 – Crack initiation and crack propagation as a percentage of total life. Baseline (SR range 400), LSP (SR 400 – 595 MPa) and LSP (400 MPa) + pit. Crack initiation is defined as a crack of 50 – 100  $\mu\text{m}$ . Due to the difficulty capturing crack initiation for LSP (SR 400MPa) samples, with and without pits, these have error bars showing an estimate of the minimum crack initiation time. Estimates are based on equivalent tests (not presented in this paper) containing corrosion pits (of approx. 50  $\mu\text{m}$  maximum. depth) and fully characterised crack propagation life.**

## 4. Discussion

### 4.1. LSP surface modification

Results in section 3.1 confirm this is a typical AA7075-T651 alloy with anisotropic microstructure and contains coarse particles typical of 7X75 aluminium alloys [38]. The large difference in number of deformed grains (captured by EBSD), particularly near the surface, clearly suggests LSP has plastically deformed the near-surface grains to at least a depth of 140  $\mu\text{m}$ . This plastic deformation causes the generation of compressive residual stresses seen in Figure 3-2. From the literature surveyed, the magnitudes of residual stress seem to be at the higher end of what has been achieved in previous LSP [39][17][40][41][42] and shot peening studies [39][43][44][45] of AA7075-T651 and other tempers [6][20].

Table 3-1 shows the LSP treatment at CSIR was successful in minimising surface roughness modification. The  $R_t$ , at 5.52  $\mu\text{m}$ , is lower than that seen in an LSP treatment with similar power density (4  $\text{GW cm}^{-2}$ ) in a key paper on LSP of AA7075 by Peyre et al. [6], where post-LSP  $R_t = 11 \mu\text{m}$  was reported. In the same study, a shot peening treatment on AA7075 performed to generate similar compressive residual stress as the current LSP treatment, produced roughness of  $R_t = 42 \mu\text{m}$ . Other studies of shot peening also show higher surface roughness on AA7075 [45][43][39].

An unintended effect of LSP treatment using an ablative coating has been the formation of small pits. As shown in Figure 3-4, pits of up to 12  $\mu\text{m}$  depth were found on LSP bend bar surfaces. Most pits were smaller than 10  $\mu\text{m}$  depth. These pits contribute to the surface roughness of the material and will act as local stress concentration features during fatigue testing. This phenomena has been reported previously by Luong and Hill [27][46], during LSP treatment of similar aluminium alloys.

Although hardness results suggest LSP increased surface hardness it is important to take into account the effect of residual stresses on hardness testing. Simes et al. [47] reports older studies, and shows, that hardness testing in loaded material (either applied or residual stresses) will over-estimate hardness values if these are compressively loaded. This agrees with the results seen in the as-received LSP samples. However, the hardness overestimation is diminished when testing cut samples. In these, the residual stress is expected to have been mostly relieved by the sample extraction process, confirming the true hardness change from LSP is likely to be limited. The way residual stress overestimates hardness is not completely clear. Simes et al. [47] study suggests the perceived hardness change is due to the residual stress modifying the stress state during hardness indentation. In contrast, Tsui et al. [48] performed a nano-indentation study that suggests the cause of overestimated values could be incorrect area deduction by material pile up. In addition, they showed once the pile-up area is taken into account, the hardness under or overestimation disappears. Thus, it is possible the apparent increase in hardness seen in the as-received LSP samples is due to area underestimation caused by material pile-up on the indent's edges.

It is difficult to compare the apparent hardness values to other studies, as these do not make it clear whether the tests take into account the residual stress effects on apparent hardness values. Hardness tests done with 25g-f by Peyre et al show limited (<10%) increase in surface hardness for AA7075-T651, which agrees with the results in this study. A key paper on LSP by Clauer [3] does not see an increase in hardness on AA7075 –T73 or T6 conditions. Clauer suggests this is due to the peak-aged alloy's high dislocation density, from precipitation hardening, limiting the ability of LSP to generate new dislocations. Longer pulse pressure duration is suggested as a way to increase dislocation density and surface hardness. Shot peening has higher pressure duration and tends to increase surface hardening more markedly [3]. An

example of this on AA7075-T6 is a study by Becker [21] which sees no increase in surface hardness for LSP AA7075-T6 and a 20% increase from shot peening; another is Zupanc and Grum [43] who see a 25% increase on AA7075-T651 after shot peening. Nevertheless, the studies do not discuss the effects of compressive residual stress on hardness testing, therefore it is not possible to assume these values are solely related to surface hardening. Taking this into consideration, the limited surface hardness increase seen on AA7075-T651 broadly correlates with what is reported in the literature.

## 4.2. Mechanistic evaluation of the effects of LSP on improving fatigue life

### 4.2.1. FE modelling

To help investigate the mechanisms underlying the experimentally observed effects of LSP on fatigue life, a finite element (FE) model was developed using ABAQUS. This model, as illustrated in Figure 4-1, represents  $\frac{1}{4}$  of the chamfered sample (Figure 2-1) used in real testing, with boundary conditions for symmetry being applied on longitudinal and transverse symmetry planes. C3D20R elements are applied in this model with a refined element thickness ranging from 0.05 – 0.1 mm in the LSP area. The rollers are modelled as rigid bodies using R3D4 elements. The contact between the rollers and the chamfered bar is assumed to be frictionless in this model. The mechanical properties of the material are represented by an isotropic material model, which was calibrated based on the monotonic true stress – strain relation of AA7075-T651.

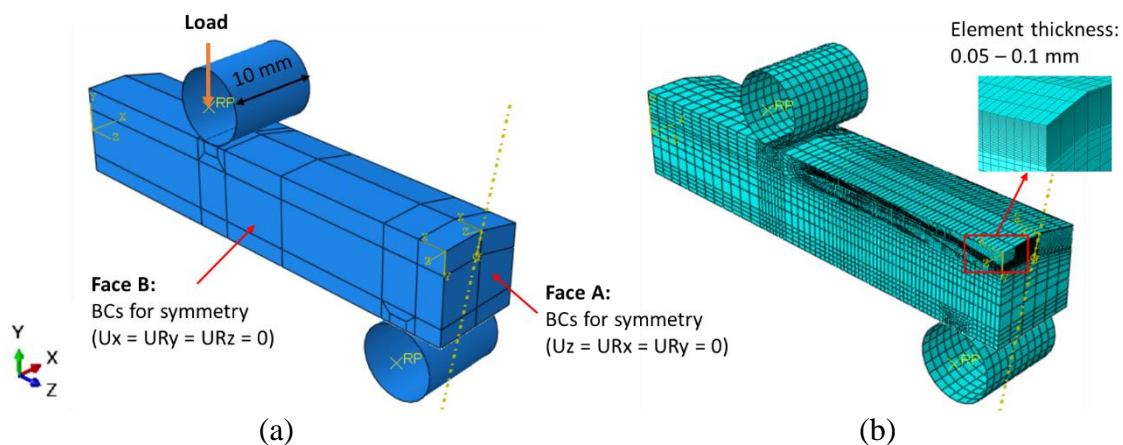


**Figure 4-1 – Finite element model of the chamfered sample with applied mesh pattern and boundary conditions: 3D view of the (a) CAD and (b) meshed model.**

The residual stresses induced by the LSP process were reconstructed in the FE model using the inverse eigenstrain method. Procedures of implementing this method are detailed in [49] hence are not repeated in detail here. The FE-reconstructed results are shown in Figure 4-2 together with the central hole drilling measurements shown in Figure 3-2, demonstrating a good consistency in the longitudinal direction ( $S_1$ ). The lower consistency in the transverse residual stress,  $S_3$ , is due to the assumed equi-biaxial eigenstrain distribution possibly being less appropriate for the chamfered area, which leads to excessive constraints in the transverse direction [49]. However, the mismatch in  $S_3$  is neglected in subsequent analysis due to the dominant role of  $S_1$  in bending fatigue behaviour.

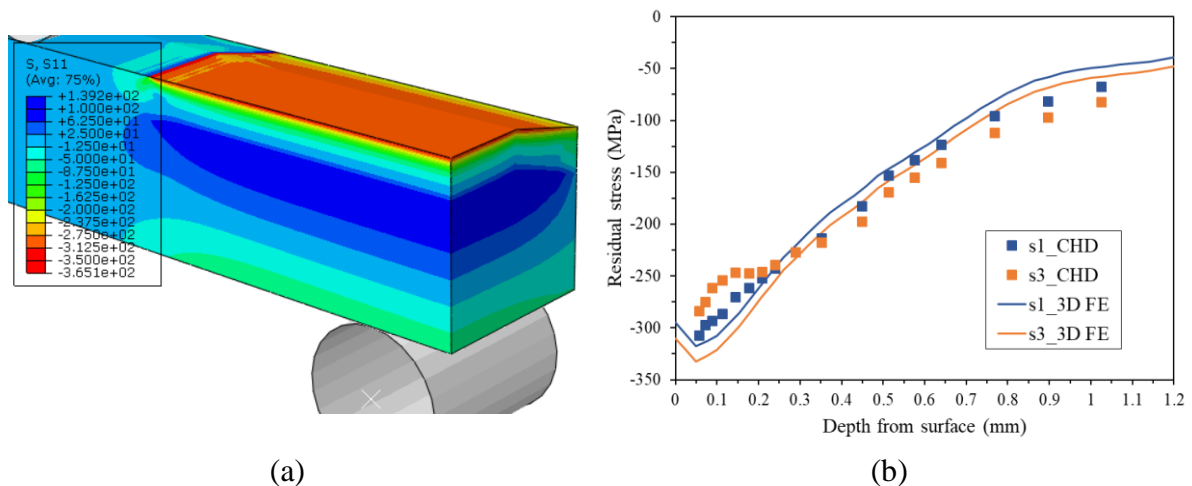


**Figure 4-2 – Reconstructed compressive residual stress distribution for the LSP sample: (a) contour plot of the longitudinal residual stress  $S_1$ , (b) comparison between the reconstructed compressive residual stress distribution with centre hole drilling (CHD) data shown in Figure 3-2.**

#### 4.2.2. Competition between surface and sub-surface crack initiation

According to Figure 3-7, there is a substantial improvement in fatigue life of samples tested at 407 MPa stress range once they have been LSP treated. In effect, LSP treatment moves fatigue performance of AA7075-T651 from the low cycle fatigue (LCF) regime to the high cycle fatigue (HCF) regime for the same applied stress range. Fractography indicates this is related to a change in the micro-mechanism of crack initiation. The LSP-induced compressive residual stress de-activates crack initiation from the coarse particles at the surface, and crack initiation

is moved subsurface (0.2 – 0.4 mm in depth), dependent only on the local stress field for initiation. To understand the associated mechanism, the mean stress distributions in baseline and LSP samples at SR 407 MPa are predicted using the FE model introduced in Section 4.2.1, and are shown in Figure 4-3(a). Clear benefits resulting from the LSP-induced compressive residual stress can be seen up to a depth of 1.0 mm, particularly at the near-surface area where the mean stress becomes negative. This implies that surface crack initiation at coarse particles in the LSP samples tends to be resisted by the surface compressive residual stress. Figure 4-3(a) further shows that the effects of the compressive residual stress start to quickly diminish with increasing depth from 0.2 mm, leading to the transition from negative to positive local mean stress. It is particularly noted that the local stress amplitude at zero mean stress point (at the depth of 0.31 mm) is 172 MPa with a local  $R = -1$ , according to the FE analysis. This stress value is greater than the fatigue limit (i.e. 159 MPa in stress amplitude) of AA7075-T651 under fully reversed uniaxial loading [31], suggesting the activation of local crack initiation and then subsequent growth. A previous study on shot peening of a high carbon chromium steel [50] showed a similar change in crack initiation mechanism from surface roughness cracks to subsurface inclusions, when shot peened. There are similarities with this study in terms of the compressive residual stress being high enough to result in the local effective cyclic stress range being low enough to not activate surface initiation at coarse particles. Unlike the aforementioned study, the present study shows coarse particles are not involved in subsequent subsurface crack initiation in the LSP samples.

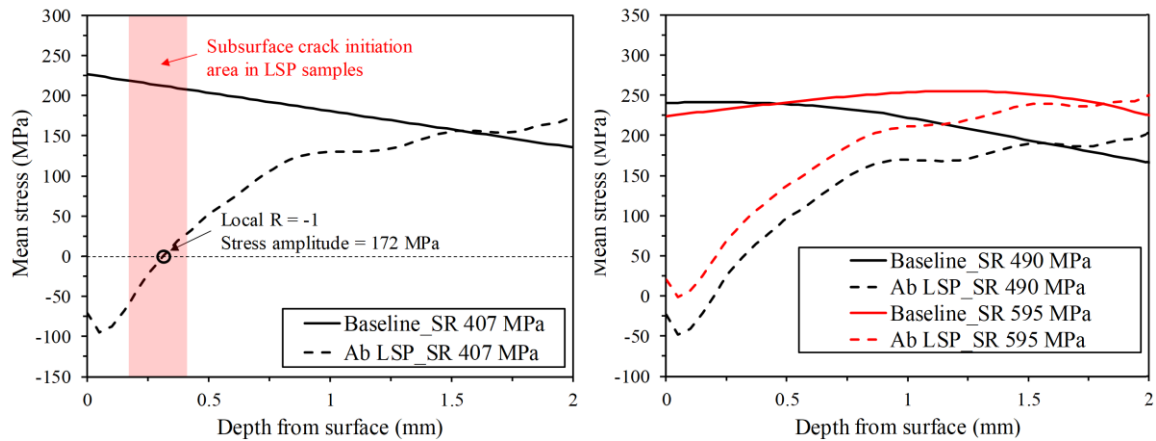


**Figure 4-3 – FE-predicted mean stress distributions in baseline and LSP samples at (a) 407 (b) 490 and 595 MPa stress ranges.**

One LSP sample tested at a stress range of 407 MPa does not behave as previous tests, dropping from the HCF regime to LCF. The cause of this drop in fatigue life is crack initiation due to a pit generated during the LSP process. Figure 3-4 shows all LSP samples have these pits, although most appear to be smaller than 10  $\mu\text{m}$ . The LSP sample tested at a stress range of 407 MPa, which failed in LCF, had an activated pit of 12  $\mu\text{m}$  depth. It is possible there is a critical depth at which a LSP process pit acts as a large enough stress concentration to overcome the effects of the compressive residual stress and suppress the LSP benefits seen in other samples. Polished LSP tests in stress ranges between 407 – 440 MPa show the effectiveness of a light polish and the removal of both surface roughness and particularly LSP process pits. It is apparent that polishing LSP samples ensures they achieve its full potential of changing it to the HCF regime and substantially increasing fatigue life. Furthermore, the test at stress range of 440 MPa shows the fatigue life for samples tested close to the yield strength of AA7075-T651 (503 MPa) can receive the full benefits of LSP. Becker [21] performed 3-point bend fatigue tests on LSP treated AA7075-T6 which saw a relatively modest improvement in fatigue life when polishing the surface, and with no change in crack initiation mechanism. These suggest that the change in crack initiation mechanism and therefore the substantial gain in fatigue life is due to a complex interplay between surface roughness and residual stress. As an interesting

example, Peyre et al. [6] fatigue tested LSP and shot peened treated AA7075-T73 and saw no subsurface cracking in the LSP samples. Compared to the present study the difference is likely due to slightly lower compressive residual stress (especially through the depth) and higher surface roughness. Shot peened AA7075-T73 on the other hand saw some subsurface crack initiation due to a combination of high compressive residual stress at the surface, very low compressive residual stress through the depth and low applied loads, despite a much higher surface roughness compared to LSP [6]. Luong and Hill performed fatigue testing on AA7050-T7451 [46], where samples had lower compressive residual stress. (approx. 250 MPa) at the surface, and higher at 0.1 mm depth (400 MPa). All cracks initiated at the surface, in some cases pits of 5 mm depth were reported as crack initiation points, and polishing the surface did not move the initiation site sub-surface, likely due to the fact that compressive residual stress were lower at the surface, promoting surface crack initiation. This in turn led to a more modest fatigue improvement in their LSP samples, and no change in fatigue regime (although several test samples, tested at lower applied loads, were stopped at one million cycles and failure mechanisms were therefore not captured).

For the fatigue test with a stress range of 490 MPa, where the maximum applied stress is above the yield strength of the material, the surface stress may be high enough to cause some plastic strain, reducing the effectiveness of any pre-existing compressive residual stress at and near the surface. The high applied stress in particular is expected to cause a return to “untreated” fatigue behaviour: crack initiation at the surface. Nevertheless, for a stress range of 490 MPa, fatigue crack initiation occurs at a pit in the bend bar chamfer, where no polishing was performed. The pit produced a high enough stress concentration to move crack initiation from the top surface to a chamfer. Further tests with a polish of all top surfaces including chamfers would be important to understand if a stress range of 490 MPa is a transition zone, or whether

at this stress range the LSP-induced compressive residual stresses are still high enough to produce HCF behaviour.

At stress ranges above the yield strength (545 – 595 MPa) all tests fail at the surface from coarse particles. This is a return to the crack initiation mechanism seen in baseline material. Figure 4-3(b) suggests that the effects of LSP-induced compressive residual stress seem to be retained at stress ranges between 490 – 595 MPa in terms of the mean stress level. Nevertheless, as shown in Figure 4-4, plastic deformation starts to accumulate in the surface layer at a stress range of 595 MPa in LSP samples, because the applied tensile stresses at the surface are too high to be compensated effectively by the compressive residual stress. This implies the transition of the crack initiation site from subsurface to the surface at high loads. Under such circumstances, the benefits of LSP tend to be greatly reduced compared to lower load levels (e.g. stress ranges between 407 – 440 MPa), as demonstrated in Figure 3-7. Surface roughness, particularly the pits as shown in Figure 3-8 (e)-(h), is also likely to further accelerate surface crack initiation, again suggesting there is a careful interplay between surface roughness (stress concentrations), applied tensile stress, and residual stress at both the surface and subsurface.

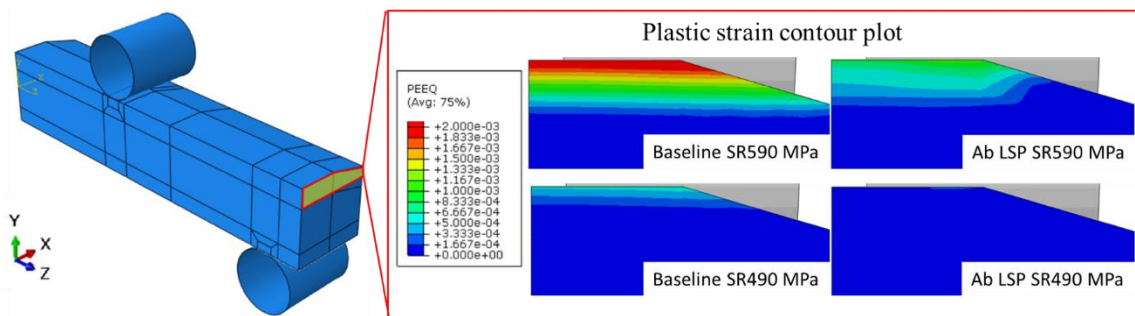


**Figure 4-4 – FE-predicted plastic strain distribution near the surface of baseline and LSP samples at SR 490 and 595 MPa (no plastic strain is generated in either baseline or LSP samples at SR 360-440 MPa).**

In terms of crack propagation determination, the beach marking method had mixed success. Particularly for LSP treated samples with sub-surface initiation. It is possible the shape of subsurface cracks (assumed semi-elliptical for the  $\Delta K$  calculation) also leads to  $\Delta K$  estimation

inaccuracies. In addition, sub-surface crack propagation within a compressive residual stress field might reduce the effectiveness of beach marking as well as the calculation of  $\Delta K$ . The LSP-induced compressive residual stress could be reducing the effectiveness of changing load ratio (R=0.1 to R=0.5) by reducing the difference in local mean  $\Delta K$ . This means the microscopic roughness that differentiates fatigue growth for different load ratios may be too similar to produce clear beach marks [51]. There is also the possibility that (due to residual stress) the local stress field goes through compressive stresses that cause contact between the two sides of the crack, which would remove beach marking evidence due to friction. This may explain why only a small number of samples had clear beach marks, and this was indeed more likely in tests where the maximum stress was above yield stress.

The LSP crack growth rate vs  $\Delta K$  data compiled suggests all LSP crack propagation is essentially within the baseline data trend. Due to the possible inaccuracies mentioned above it is possible that any crack growth rate delay by LSP is underestimated. The existing deep compressive residual stress in the samples would be expected to delay crack propagation. Previous literature [6] suggest this would be the case for AA7075-T651 and that LSP would slow crack propagation but this will probably be a small contribution to overall fatigue life improvement. In addition, Figure 3-11 shows LSP-induced compressive residual stress vastly increases initiation time, but this also depends on the applied stress range. The higher the applied stress range, the less effective LSP-induced compressive residual stress are at delaying crack initiation. In addition, the LSP-induced residual stress field and depth profile, as well as the shape and depth of defects (including pits) appear to be important variables influencing fatigue crack initiation mechanisms (surface or sub-surface) and thus changes in fatigue regime. Thus, the main conclusion that can be taken from this study's crack growth data is that crack initiation is the main cause of the observed fatigue life increase. There is likely to be an improvement in crack propagation but this is assumed relatively small compared to crack

initiation and has been hard to determine explicitly. Further work is required to accurately capture crack propagation data (short crack shape, growth rate and  $\Delta K$ ) in LSP samples under high cycle fatigue. One possibility being considered is using X-ray tomography (ex- and / or in-situ) in combination with other characterisation techniques (SEM, FIB), as this has been shown to produce high resolution data of fatigue cracks and surrounding microstructure [52][53][54].

## 5. Conclusions

The following conclusions can be drawn from this study:

1. An LSP treatment set up to maximise compressive residual stresses whilst minimising surface modification was successful in vastly improving fatigue performance of AA7075-T651.
2. The largest improvement in fatigue performance is for cases where the maximum applied stresses were below the yield strength of AA7075-T651, and where a change was observed in fatigue crack initiation mechanism (from surface coarse particles for baseline, to subsurface and dependent on the local stress field for LSP). This transition also pushed the fatigue behaviour into the high cycle fatigue regime.
3. At high loads, where maximum applied stresses were above the yield strength, the combination of high applied loads and plastic strain at the surface relieve the LSP compressive residual stress benefits. This returned the observed fatigue behaviour to the low cycle fatigue regime, where coarse particles at the surface are the main crack initiation sites. Thus, fatigue life improvement from LSP is small under these loading conditions.
4. An increase in crack propagation time for LSP treated samples is expected but appears relatively small compared to the much larger increase observed in crack initiation time (at the same nominal applied stress ranges). The increase in crack propagation time is expected, however characterising is very challenging with the techniques used in this study.
5. The surface condition of the material is critical to obtaining the maximum benefits from LSP compressive residual stresses. More investigation is required to understand the interplay between a critical depth at which a surface feature acts as a stress concentration and counteracts a given LSP-induced compressive residuals stress profile

enough to prevent a change to sub-surface crack initiation, drastically reducing the potential for increased fatigue performance.

## 6. Acknowledgements

This study is financially supported by the Engineering and Physical Sciences Research Council (EPSRC). The authors would like to acknowledge the funding and support of the University of Southampton. The support of Coventry University for performing residual stress analysis and providing laser shock peening expertise. The Council of Scientific and Industrial Research (CSIR) of South Africa for access to laser shock peening equipment and expertise. The financial support and sponsorship by Airbus Operations GmbH.

Michael E. Fitzpatrick is grateful for funding from the Lloyd's Register Foundation, a charitable foundation helping protect life and property by supporting engineering-related education, public engagement, and the application of research.

## 7. References

- [1] K. Ding and L. Ye, “General introduction,” in *Laser Shock Peening*, Elsevier, 2006, pp. 1–6.
- [2] B. P. Fairand and A. H. Clauer, “APPLICATIONS OF LASER-INDUCED STRESS WAVES,” The Society of Manufacturing Engineers, Cambridge, Massachusetts, 1978. Accessed: Jun. 24, 2018. [Online]. Available: <https://www.lsptechnologies.com/wp-content/uploads/2008/05/pub1007.pdf>.
- [3] A. H. Clauer, J. H. Holbrook, and B. P. Fairand, *EFFECTS OF LASER INDUCED SHOCK WAVES ON METALS*. New York: Plenum Publishing Corporation, 1981.
- [4] A. H. Clauer, “Laser Shock Peening for Fatigue Resistance,” *Surface Performance of Titanium*, no. 1996, pp. 217–230, 1996, doi: 10.1007/BF00414201.
- [5] P. Peyre, R. Fabbro, L. Berthe, and C. Dubouchet, “Laser shock processing of materials, physical processes involved and examples of applications,” *Journal of Laser Applications*, vol. 8, no. 3, pp. 135–141, 1996.
- [6] P. Peyre, R. Fabbro, P. Merrien, and H. P. Lieurade, “Laser shock processing of aluminium alloys. Application to high cycle fatigue behaviour,” *Materials Science and Engineering: A*, vol. 210, no. 1–2, pp. 102–113, Jun. 1996, doi: 10.1016/0921-5093(95)10084-9.
- [7] M. Newby, A. Steuwer, D. Glaser, C. Polese, D. G. Hattingh, and C. Gorny, “Synchrotron XRD Evaluation of Residual Stresses Introduced by Laser Shock Peening for Steam Turbine Blade Applications,” in *Mechanical Stress Evaluation by Neutron and Synchrotron Radiation*, May 2018, vol. 4, pp. 97–102, doi: 10.21741/9781945291678-15.
- [8] M. Dorman, M. B. Toparli, N. Smyth, A. Cini, M. E. Fitzpatrick, and P. E. Irving, “Effect of laser shock peening on residual stress and fatigue life of clad 2024 aluminium

- sheet containing scribe defects,” *Materials Science and Engineering A*, vol. 548, pp. 142–151, Jun. 2012, doi: 10.1016/j.msea.2012.04.002.
- [9] A. H. Clauer, C. T. Walters, and S. C. Ford, “The Effects of Laser Shock Processing on the Fatigue Properties of 2024-T3 Aluminum | Request PDF,” in *ASM Conference on Lasers in Materials Processing*, 1986, pp. 7–22, Accessed: Apr. 03, 2020. [Online]. Available:  
[https://www.researchgate.net/publication/283967984\\_The\\_Effects\\_of\\_Laser\\_Shock\\_Processing\\_on\\_the\\_Fatigue\\_Properties\\_of\\_2024-T3\\_Aluminum](https://www.researchgate.net/publication/283967984_The_Effects_of_Laser_Shock_Processing_on_the_Fatigue_Properties_of_2024-T3_Aluminum).
- [10] S. Zabeen, K. Langer, and M. E. Fitzpatrick, “Effect of alloy temper on surface modification of aluminium 2024 by laser shock peening,” *Surface and Coatings Technology*, vol. 347, no. March, pp. 123–135, 2018, doi: 10.1016/j.surfcoat.2018.04.069.
- [11] M. Abeens, R. Muruganandhan, K. Thirumavalavan, and S. Kalainathan, “Surface modification of AA7075 T651 by laser shock peening to improve the wear characteristics,” *Materials Research Express*, vol. 6, no. 6, pp. 1–13, Mar. 2019, doi: 10.1088/2053-1591/ab0b0e.
- [12] Q. Liu, “An Effective Life Extension Technology for 7xxx Series Aluminium Alloys by Laser Shock Peening (Final Report),” Victoria, Australia, 2008. Accessed: Nov. 27, 2018. [Online]. Available:  
<http://citeseerx.ist.psu.edu/viewdoc/download?doi=10.1.1.427.4977&rep=rep1&type=pdf>.
- [13] Q. Liu, S. Barter, and G. Clark, “Internal cracking during surface treatment of 7050-T74 aluminium alloy using laser shock peening,” *Structural Integrity and Fracture: Proceedings of the International Conference, SIF 2002, Perth, Australia, 25-28 September 2002*, p. 177, 2002.

- [14] F. J. Carpio, D. Araújo, F. J. Pacheco, D. Méndez, A. J. García, M. P. Villar, R. García, D. Jiménez, and L. Rubio, "Fatigue behaviour of laser machined 2024 T3 aeronautic aluminium alloy," *Applied Surface Science*, vol. 208–209, no. 1, pp. 194–198, Mar. 2003, doi: 10.1016/S0169-4332(02)01369-7.
- [15] J. Grum, U. Trdan, and M. R. Hill, "Laser shock processing of ENAW 6082 aluminium alloy surface," *Materials Science Forum*, vol. 589, pp. 379–384, 2008, doi: 10.4028/www.scientific.net/msf.589.379.
- [16] Z. Yongkang, Z. Shuyi, Z. Xiaorong, C. Lan, Y. Jichang, and R. Naifei, "Investigation of the surface qualities of laser shock-processed zones and the effect on fatigue life of aluminum alloy," *Surface and Coatings Technology*, vol. 92, no. 1–2, pp. 104–109, Jun. 1997, doi: 10.1016/S0257-8972(97)00009-1.
- [17] X. Q. Q. Zhang, H. Li, X. L. L. Yu, Y. Zhou, S. W. W. Duan, S. Z. Z. Li, Z. L. L. Huang, and L. S. S. Zuo, "Investigation on effect of laser shock processing on fatigue crack initiation and its growth in aluminum alloy plate," *Materials & Design (1980-2015)*, vol. 65, pp. 425–431, Jan. 2015, doi: 10.1016/J.MATDES.2014.09.001.
- [18] S. Gencalp Irizalp, N. Saklakoglu, E. Akman, and A. Demir, "Pulsed Nd: YAG laser shock processing effects on mechanical properties of 6061-T6 alloy," *Optics and Laser Technology*, vol. 56, pp. 273–277, Mar. 2014, doi: 10.1016/j.optlastec.2013.08.011.
- [19] U. Trdan, J. L. Ocaña, and J. Grum, "Surface Modification of Aluminium Alloys with Laser Shock Processing," *Journal of mechanical engineering*, vol. 57, no. 5, pp. 385–393, 2010, doi: 10.5545/sv-jme.2010.119.
- [20] G. Ivetic, I. Meneghin, E. Troiani, G. Molinari, A. Lanciotti, V. Ristori, J. L. Ocaña, M. Morales, J. A. Porro, C. Polese, and A. M. Venter, "Characterisation of fatigue and crack propagation in laser shock peened open hole 7075-T73 aluminium specimens," in *ICAF 2011 Structural Integrity: Influence of Efficiency and Green Imperatives - Proceedings*

- of the 26th Symposium of the International Committee on Aeronautical Fatigue, 2011, pp. 855–866, doi: 10.1007/978-94-007-1664-3\_66.
- [21] A. Becker, “The Effect of Laser Shock Peening and Shot Peening on the Fatigue Performance of Aluminium Alloy 7075,” University of Cape Town, 2017.
- [22] Y. K. Gao, “Improvement of fatigue property in 7050–T7451 aluminum alloy by laser peening and shot peening,” *Materials Science and Engineering: A*, vol. 528, no. 10–11, pp. 3823–3828, Apr. 2011, doi: 10.1016/J.MSEA.2011.01.077.
- [23] A. M. Mostafa, M. F. Hameed, and S. S. Obayya, “Effect of laser shock peening on the hardness of AL-7075 alloy,” *Journal of King Saud University - Science*, vol. 31, no. 4, pp. 472–478, Oct. 2019, doi: 10.1016/j.jksus.2017.07.012.
- [24] A. H. Clauer, “Laser shock processing increases fatigue life of metal parts,” *Materials and processing report*, vol. 6, no. 6, pp. 3–5, 1991.
- [25] O. Hatamleh, J. Lyons, and R. Forman, “Laser peening and shot peening effects on fatigue life and surface roughness of friction stir welded 7075-T7351 aluminum,” *Fatigue and Fracture of Engineering Materials and Structures*, vol. 30, no. 2, pp. 115–130, 2007, doi: 10.1111/j.1460-2695.2006.01093.x.
- [26] ASM Aerospace Specification Metals Inc., “Aluminium 7075-T6; 7075-T651,” *MatWeb*, 2001. <http://asm.matweb.com/search/SpecificMaterial.asp?bassnum=MA7075T6> (accessed Jan. 03, 2020).
- [27] H. Luong and M. R. Hill, “The effects of laser peening on high-cycle fatigue in 7085-T7651 aluminum alloy,” *Materials Science and Engineering A*, vol. 477, no. 1–2, pp. 208–216, 2008, doi: 10.1016/j.msea.2007.05.024.
- [28] University of Columbia, *Practical residual stress measurement methods*, 1st ed., vol. 1, no. 1. Vancouver: University of Columbia, 2013.

- [29] Oxford Instruments HKL, "CHANNEL 5," Denmark, 2007.
- [30] F. Bachmann, R. Hielscher, and H. Schaeben, "Grain detection from 2d and 3d EBSD data-Specification of the MTEX algorithm," *Ultramicroscopy*, vol. 111, no. 12, pp. 1720–1733, Dec. 2011, doi: 10.1016/j.ultramic.2011.08.002.
- [31] P. V Grant, J. D. Lord, P. S. Whitehead, National Physics Laboratory, and S. Ltd, "The Measurement of Residual Stresses by the Incremental Hole Drilling Technique," *Measurement Good Practice Guide*, vol. 53, no. 2, p. 63, 2006.
- [32] D. Glaser, M. Newby, C. Polese, L. Berthe, A. M. Venter, D. Marais, N. J.P., G. Styger, S. Paddea, and S. N. van Staden, "Evaluation of Residual Stresses Introduced by Laser Shock Peening in Steel using Different Measurement Techniques," in *Mechanical Stress Evaluation by Neutron and Synchrotron Radiation*, May 2018, vol. 4, pp. 45–50, doi: 10.21741/9781945291678-7.
- [33] N. E. Dowling, C. A. Calhoun, and A. Arcari, "Mean stress effects in stress-life fatigue and the Walker equation," *Fatigue and Fracture of Engineering Materials and Structures*, vol. 32, no. 3, pp. 163–179, Mar. 2009, doi: 10.1111/j.1460-2695.2008.01322.x.
- [34] T. Zhao and Y. Jiang, "Fatigue of 7075-T651 aluminum alloy," *International Journal of Fatigue*, vol. 30, no. 5, pp. 834–849, 2008, doi: 10.1016/j.ijfatigue.2007.07.005.
- [35] J. Schindelin, I. Arganda-Carreras, E. Frise, V. Kaynig, M. Longair, T. Pietzsch, S. Preibisch, C. Rueden, S. Saalfeld, B. Schmid, J.-Y. Tinevez, D. J. White, V. Hartenstein, K. Eliceiri, P. Tomancak, and A. Cardona, "Fiji: an open-source platform for biological-image analysis," *Nature Methods*, vol. 9, no. 7, pp. 676–682, Jul. 2012, doi: 10.1038/nmeth.2019.
- [36] Y. Jin, P. Cai, W. Wen, H. Nagaumi, B. Xu, Y. Zhang, and T. Zhai, "The anisotropy of fatigue crack nucleation in an AA7075 T651 Al alloy plate," *Materials Science and*

- Engineering A*, vol. 622, pp. 7–15, 2015, doi: 10.1016/j.msea.2014.11.007.
- [37] A. Rohatgi, “WebPlotDigitizer,” 2015. <https://automeris.io/WebPlotDigitizer>.
- [38] N. Birbilis and R. G. Buchheit, “Electrochemical Characteristics of Intermetallic Phases in Aluminum Alloys,” *Journal of The Electrochemical Society*, vol. 152, no. 4, p. B140, 2005, doi: 10.1149/1.1869984.
- [39] M. Mhaede, Y. Sano, I. Altenberger, and L. Wagner, “Fatigue Performance of Al7075-T73 and Ti-6Al-4V : Comparing Results after Shot Peening , Laser Shock Peening and Ball- Burnishing,” *Proc. Shot peening - ICSP11*, pp. 2–7, 2011.
- [40] J. T. Wang, Y. K. Zhang, J. F. Chen, J. Y. Zhou, K. Y. Luo, W. S. Tan, L. Y. Sun, and Y. L. Lu, “Effect of laser shock peening on the high-temperature fatigue performance of 7075 aluminum alloy,” *Materials Science and Engineering A*, vol. 704, pp. 459–468, Sep. 2017, doi: 10.1016/j.msea.2017.08.050.
- [41] H. Wang, C. Ning, Y. Huang, Z. Cao, X. Chen, and W. Zhang, “Improvement of abrasion resistance in artificial seawater and corrosion resistance in NaCl solution of 7075 aluminum alloy processed by laser shock peening,” *Optics and Lasers in Engineering*, vol. 90, pp. 179–185, Mar. 2017, doi: 10.1016/j.optlaseng.2016.10.016.
- [42] J. T. Wang, Y. K. Zhang, J. F. Chen, J. Y. Zhou, M. Z. Ge, Y. L. Lu, and X. L. Li, “Effects of laser shock peening on stress corrosion behavior of 7075 aluminum alloy laser welded joints,” *Materials Science and Engineering A*, vol. 647, pp. 7–14, Oct. 2015, doi: 10.1016/j.msea.2015.08.084.
- [43] U. Zupanc and J. Grum, “Surface integrity of shot peened aluminium alloy 7075-T651,” *Strojniski Vestnik/Journal of Mechanical Engineering*, vol. 57, no. 5, pp. 379–384, 2011, doi: 10.5545/sv-jme.2010.142.
- [44] V. Pandey, J. K. K. Singh, K. Chattopadhyay, N. C. C. S. S. Srinivas, and V. Singh, “Influence of ultrasonic shot peening on corrosion behavior of 7075 aluminum alloy,”

- Journal of Alloys and Compounds*, vol. 723, pp. 826–840, Nov. 2017, doi: 10.1016/j.jallcom.2017.06.310.
- [45] S. Zagar and J. Grum, “Roughness, residual stresses and pitting corrosion effect on shot peened AA 7075,” *Technical Gazette*, vol. 22, no. 6, pp. 1589–1595, 2015, doi: 10.17559/TV.
- [46] H. Luong and M. R. Hill, “The effects of laser peening and shot peening on high cycle fatigue in 7050-T7451 aluminum alloy,” *Materials Science and Engineering A*, vol. 527, no. 3, pp. 699–707, 2010, doi: 10.1016/j.msea.2009.08.045.
- [47] T. R. Simes, S. G. Mellor, and D. A. Hills, “A note on the influence of residual stress on measured hardness,” *The Journal of Strain Analysis for Engineering Design*, vol. 19, no. 2, pp. 135–137, Apr. 1984, doi: 10.1243/03093247V192135.
- [48] T. Y. Tsui, W. C. Oliver, and G. M. Pharr, “Influences of stress on the measurement of mechanical properties using nanoindentation: Part I. Experimental studies in an aluminum alloy,” *Journal of Materials Research*, vol. 11, no. 3, pp. 752–759, 1996, doi: 10.1557/JMR.1996.0091.
- [49] C. You, M. Achintha, K. A. Soady, N. Smyth, M. E. Fitzpatrick, and P. A. S. Reed, “Low cycle fatigue life prediction in shot-peened components of different geometries—part I: residual stress relaxation,” *Fatigue & Fracture of Engineering Materials & Structures*, vol. 40, no. 5, pp. 761–775, May 2017, doi: 10.1111/ffe.12543.
- [50] K. Shiozawa, Y. Morii, S. Nishino, and L. Lu, “Subsurface crack initiation and propagation mechanism in high-strength steel in a very high cycle fatigue regime,” *International Journal of Fatigue*, vol. 28, no. 11, pp. 1521–1532, Nov. 2006, doi: 10.1016/j.ijfatigue.2005.08.015.
- [51] S. P. Lynch, “Progression markings, striations, and crack-arrest markings on fracture surfaces,” *Materials Science and Engineering A*, vol. 468–470, no. SPEC. ISS., pp. 74–

- 80, Nov. 2007, doi: 10.1016/j.msea.2006.09.083.
- [52] T. J. Stannard, J. J. Williams, S. S. Singh, A. S. Sundaram Singaravelu, X. Xiao, and N. Chawla, “3D time-resolved observations of corrosion and corrosion-fatigue crack initiation and growth in peak-aged Al 7075 using synchrotron X-ray tomography,” *Corrosion Science*, vol. 138, pp. 340–352, Jul. 2018, doi: 10.1016/j.corsci.2018.04.029.
- [53] A. S. S. Singaravelu, J. J. Williams, H. D. Goyal, S. Niverty, S. S. Singh, T. J. Stannard, X. Xiao, and N. Chawla, “3D Time-Resolved Observations of Fatigue Crack Initiation and Growth from Corrosion Pits in Al 7XXX Alloys Using In Situ Synchrotron X-ray Tomography,” *Metallurgical and Materials Transactions A: Physical Metallurgy and Materials Science*, vol. 51, no. 1, pp. 28–41, Jan. 2020, doi: 10.1007/s11661-019-05519-z.
- [54] B. Y. He, K. a Soady, B. G. Mellor, a Morris, and P. a S. Reed, “Effects of shot peening on short crack growth rate and resulting low cycle fatigue behaviour in low pressure turbine blade material,” *Materials Science and Technology*, vol. 29, no. 7, pp. 788–796, 2013, doi: 10.1179/1743284713Y.0000000230.

## I. List of Figures

Figure 2-1 .- Schematics of AA7075-T651 plate and LSP sample geometry and LSP area. ....	8
Figure 3-1 – Top left: 3-D representation of AA7075-T651 microstructural planes.....	14
Figure 3-2 - Centre hole drilling data for LSP samples. $S_1$ in the longitudinal direction, $S_3$ in the transverse direction. ....	15
Figure 3-3 – Vickers micro-hardness measurements of baseline LSP samples.....	16
Figure 3-4 – An example of a bend bar surface with pits generated by LSP process. Number of pits per area differs greatly but is generally considered low. Captured by variable focus microscopy.....	17
Figure 3-5 – EBSD maps of samples cross-sections, LT-ST plane. Surface at the bottom, upwards going away from surface. Left: Baseline. Right: LSP.....	18
Figure 3-6 – Top: Recrystallised fraction graph of baseline and LSP surface for LT-ST cross sections: 0 – 140 $\mu\text{m}$ away from surface. Bottom: Kernel average misorientation vs. distance away from LSP surface. ....	19
Figure 3-7 – Stress vs. number of fatigue cycles (S-N) curve. Literature values taken from Jin et al. [36] using WebPlotDigitizer open source software [37]. Erros bars account for fatigue life estimate and variation due to change of load ratio during cycling. ....	21
Figure 3-8 – Low and high magnification images of crack initiation sites for different fatigue test conditions. a-b: All baseline tests. c-d: LSP tests at 407 MPa stress range. e-f: One LSP test at 407 MPa which was an exception to the previous tests. g-h: LSP test at 490 MPa stress range. i-j: LSP tests at or above 545 MPa stress range. ....	23
Figure 3-9 – Topographical images of both sides of pit acting as initiation site of LSP bend bar. Tested at 407 MPa stress range. Failed at $10^5$ cycles. Taken from top surface (L-LT plane). ....	24

Figure 3-10 – Crack growth data vs. stress intensity factor for baseline and LSP fatigue tested samples. This includes crack propagation data captured by replica method and the beach marking method. ....25

Figure 3-11 – Crack initiation and crack propagation as a percentage of total life. Baseline (SR range 400), LSP (SR 400 – 595 MPa) and LSP (400 MPa) + pit. Crack initiation is defined as a crack of 50 – 100  $\mu\text{m}$ . Due to the difficulty capturing crack initiation for LSP (SR 400MPa) samples, with and without pits, these have error bars showing an estimate of the minimum crack initiation time. Estimates are based on equivalent tests (not presented in this paper) containing corrosion pits (of approx. 50  $\mu\text{m}$  maximum. depth) and fully characterised crack propagation life. ....26

Figure 4-1 – Finite element model of the chamfered sample with applied mesh pattern and boundary conditions: 3D view of the (a) CAD and (b) meshed model. ....30

Figure 4-2 – Reconstructed compressive residual stress distribution for the LSP sample: (a) contour plot of the longitudinal residual stress  $S_1$ , (b) comparison between the reconstructed compressive residual stress distribution with centre hole drilling (CHD) data shown in Figure 3-2. ....30

Figure 4-3 – FE-predicted mean stress distributions in baseline and LSP samples at (a) 407 (b) 490 and 595 MPa stress ranges. ....31

Figure 4-4 – FE-predicted plastic strain distribution near the surface of baseline and LSP samples at SR 490 and 595 MPa (no plastic strain is generated in either baseline or LSP samples at SR 360-440 MPa).....31

## II. List of Tables

Table 2-1 – LSP parameters.....8

Table 2-2 – Electropolishing parameters ..... 10

Table 3-1 – Average roughness measurements for baseline and as received LSP. .... 16